Potential Gas Generation in a Salt Repository

Gas Generation Model – Functional Specification and Definition of Central Case for Analysis

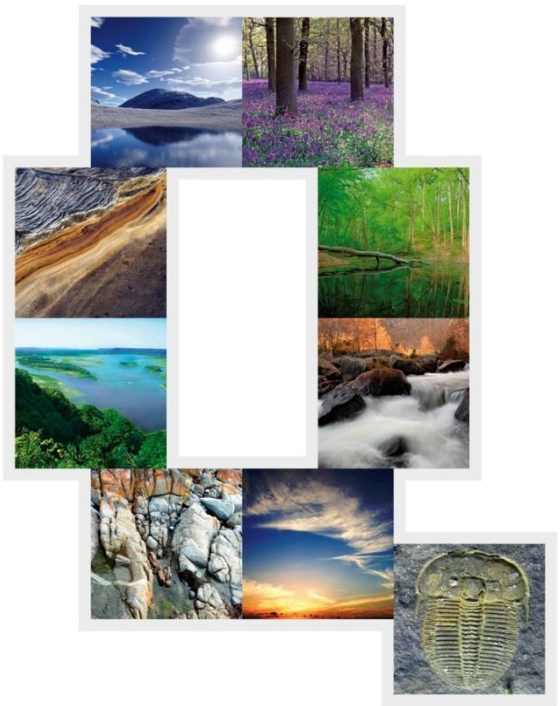

S Benbow, R Newson,
L Bruffell, A Bond, S Watson

QDS-10075A-T2-FS
Version 1

February 2023

Quintessa

Document Details

Quintessa Document Owner: S Benbow
Client: COVRA
Security Status: Public

Document History

Version	Date	Changes	Editor(s)	Reviewer(s)	Approver
1	15/02/2023		S Benbow	S Watson, J Bartol	A Bond

Quintessa Limited
First Floor, West Wing
Videcom House, Newtown Road
Henley-on-Thames
Oxfordshire RG9 1HG
United Kingdom

Tel: +44 (0) 1491 636246
info@quintessa.org
www.quintessa.org

An employee-owned company
Registration No. 3716623

Summary

A high-level conceptualisation of potential gas generation processes in COVRA's OPERA Safety Case (Verhoef et al., 2017) is given by Watson (2023).

This report presents a functional specification for a simple model for estimating amounts and timescales associated with gas generation from a single waste package based on the conceptualisation provided by Watson (2023). Only gas generation from waste packages, and not the overpacks is considered in the model. The overpack is being considered separately by COVRA in another study.

Parameter values to represent a central case for analysis based on best estimates of waste inventories and package geometries from the OPERA reports and tunnel void spaces determined from separate information provided by COVRA are also given, together with general parameters for determining rates of gas generation due to corrosion, organic degradation and radiolysis.

Verification of the central analysis case calculations by comparison of the results obtained from two independently developed implementations of the gas generation model using Quintessa's QPAC software (Quintessa, 2013) and the GoldSim ® software (GTG, 2017) is presented. The QPAC version of the model is used in the accompanying modelling report (Benbow et al., 2023).

Contents

1 Introduction

A high-level conceptualisation of potential gas generation processes in COVRA's OPERA Safety Case (Verhoef et al., 2017) is given by Watson (2023).

This report presents a functional specification for a simple model for estimating amounts and timescales associated with gas generation from a single waste package based on the conceptualisation provided by Watson (2023). Parameter values to represent a central case for analysis based on best estimates of waste inventories and package geometries from the OPERA reports and package and tunnel void spaces determined from separate information provided by COVRA are also given, together with general parameters for determining rates of gas generation due to corrosion, organic degradation and radiolysis. Only gas generation from waste packages, and not the overpacks is considered in the model. The overpack is being considered separately by COVRA in another study. It is only accounted for in the model presented here by sensitivity cases that delay the arrival of water (brine) from the geosphere to represent protection from the overpack.

The gas generation model is composed of two parts: a package-scale gas generation model and a storage and disposal scenario model. The package-scale gas generation model includes gas generation from corrosion, organic degradation and radiolysis processes that can occur in a single waste package during the storage/operational and post-closure phases. The storage and disposal scenario model describes the environmental conditions affecting a collection of similar waste packages first during the storage phase and then after emplacement in and closure of the disposal tunnel, including details such as the duration in storage and the post-closure water availability.

The storage and disposal scenario model is described in Section 2 and the package-scale gas generation model is described in Section 3. In each section, tables of input parameters are given that characterise the scenario/package for each of the waste groups that are considered. Input parameter values that are given represent indicative central analysis case values. Model reaction rate parameters that are independent of the waste group or scenario are given in Appendices A-C. Appendix D gives details of verification that has been performed for independently developed implementations of the gas generation model using Quintessa's QPAC software (Quintessa, 2013) and the GoldSim ® software (GTG, 2017). The QPAC version of the model is used in the accompanying modelling report (Benbow et al., 2023), which presents results for the central analysis case parameterisation of the model and a selection of sensitivity analysis cases.

2 Storage and Disposal Scenario Model

Waste packages are assumed to be placed in storage at some time t_s (y) and then be moved and emplaced in the repository at a later time t_r (y).

Treatment of availability of water will be a strong control on the overall analysis of gas generation. Sources of water comprise initial water that is incorporated into the waste and encapsulants, and, after closure, water (brine) that is initially present in the backfill and near-field and water that enters the repository from the geosphere. Water approaching from the backfill and geosphere will come into contact with waste package outer surfaces after the overpack has failed (if it is watertight), although as noted in Section 1, the overpack is not explicitly represented in the current modelling, except in sensitivity cases that delay the arrival of water from the backfill and geosphere to represent protection from the overpack. A fraction of the incoming water may directly enter packages if they are open or vented. Otherwise, water will only enter the packages and contact the waste once the package outer surface is corroded or fails mechanically (e.g. due to loading from salt creep or tunnel collapse). Water that is in contact with the waste inside the package may be subject to α, β and γ radiolysis and water outside the package may be subject to γ radiolysis, depending on the waste type.

Water arriving from the geosphere will first encounter overpacks (where relevant) before encountering waste packages. Therefore, the coupling assumed between the models of overpack corrosion, which are being investigated by COVRA in separate studies, and the models of waste package corrosion that are considered here will affect the estimated total rates and amounts of generated gas. A detailed treatment of this coupling of water availability is beyond the scope of the current study. Modelling it would require coupling the gas generation model with a hydrogeological model of flows of water and gas in the near field and nearby host rock of the type performed by Watson et al. (2012). In the current models, the rate of supply of water to the waste packages is an input parameter that should be chosen considering rates of water supply from the geosphere and consumption in the overpack corrosion processes.

The scenario model defines the rate at which water approaches the waste package from the geosphere, after consideration of any water consumption in interactions with any overpack, and the *initial* fraction of the water that enters the package. These are denoted by $Q_{geo}(t)$ (mol/y) and $f_{pkg,init}$ (-) respectively. $f_{pkg,init}$ will usually be zero for sealed packages, unless considering an initial defect scenario. The imposed time of mechanical failure of the package (if any) is denoted $t_{pkg,fail}$ (y), after which time the fraction of the approaching water that enters the package changes to $f_{pkg,fail}$ (-). The package scale model monitors the amount of uncorroded external waste packaging and after total corrosion of the external packaging all approaching water is assumed to enter the package (Section 3.1).

The composition of the water approaching the package can be in one of eight states, one for each combination of oxic/anoxic, low/high chloride, neutral/alkaline conditions.

Water approaching the exterior of the package (i.e. that water that does not pass directly into the package) will reside in the pore/void volume adjacent to the waste package until it is consumed in corrosion reactions with the package outer surface or by radiolysis. The available pore/void volume, which may vary with time due to salt creep, is denoted $V_{out}^{P}(t)$ (m^3). In the central analysis case calculations, this volume is held constant. This pore/void volume is assumed to have an initial water saturation of S_{out}^{W} (-) at time t_r and reside in a mass of solid, $M_{surround}$ (kg). This mass is required in the calculation of gas generation due to radiolysis outside of the package (Section 3.3). If the solid represented by the volume adjacent to the package is cementitious then this will be assumed to condition the water to alkaline before it enters the package or encounters the outer package surface.

Rates of water infiltration toward the waste packages are not known. To derive plausible flow rates for Q_{geo} a notional water availability in terms of a mass rate of water per unit length of disposal tunnel is imposed. In the central analysis case models this rate is chosen to be 1 g/m/day. Combining this with the number of waste packages per unit tunnel length allows representative values for Q_{geo} to be determined.

The water availability rate of 1 g/m/day is based on work undertaken in the DECOVALEX 2023 programme (Guiltinan et al., 2022), where models of inflow to open tunnels in the bedded salt at WIPP were developed. The estimated inflows ranged between 6 and 60 g/m/day for a "drying down" scenario in which the tunnel engineering damaged zone (EDZ) was assumed to be initially fully saturated, but were found to be 100 smaller when a "wetting up" scenario was considered in which the EDZ was assumed to be initially relatively dry. The current Dutch disposal concept is in a domal salt formation, which tend to be drier than bedded salts, although the potential for a repository in bedded salt, which is also found in the Netherlands, has not been discounted. The chosen value of 1 g/m/day is close to the logarithmic mean of the estimated range of WIPP inflows. In the case of WIPP, maintaining an atmospheric boundary condition leads to continued flows into the repository. In the context of the current modelling, continued consumption of water in gas-generating processes performs a similar role, so in the absence of other information a continuing water inflow is assumed.

It is noted that pressurisation of the excavation, which might be expected to restrict water inflow, and eventually shut it down, is conservatively ignored in the central analysis case. Since Q_{geo} can be imposed on the model as a function of time, gradual restriction of inflow can be represented if a suitable timescale is known.

The number of packages per unit tunnel length and the void space around each package is calculated based on cross-section diagrams, shown in Figure 2-1 and Figure 2-2. The

number of packages per unit tunnel length is taken to be the number of packages in the tunnel (disposal room) divided by the tunnel length (100m in the lower level, and 90m in the upper level). The number of packages in each tunnel in the lower level is the number of containers (10) multiplied by the number of packages per container (6 in the CSD-V and CSD-C containers, and 2 in the ECN container). The numbers of packages in each tunnel in the upper level are taken from the cross sections shown in Figure 2-2, and for the DDS container, it is assumed that in a single disposal room there will be 15 rows of 14 containers, each stacked 4 high (to give a total of 840 per room).

The void space around each package is calculated to be the total void space in the tunnel (the volume of the packages subtracted from the volume of the tunnel), divided by the number of packages. In the lower level, only half of the volume of the packages is subtracted from the tunnel volume, since they are assumed to be sunk into the tunnel floor, up to half of their height, as shown in Figure 2-1. The void space is assumed to be backfilled with crushed salt with a porosity of 0.33 when computing the net void volume V_{out}^{P}.

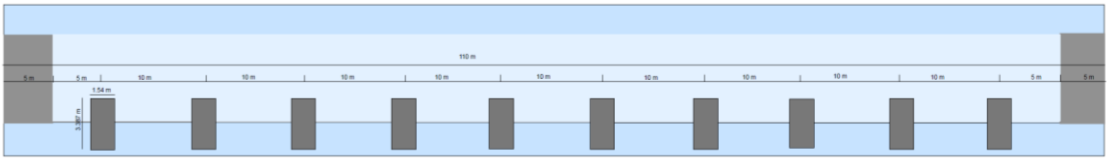

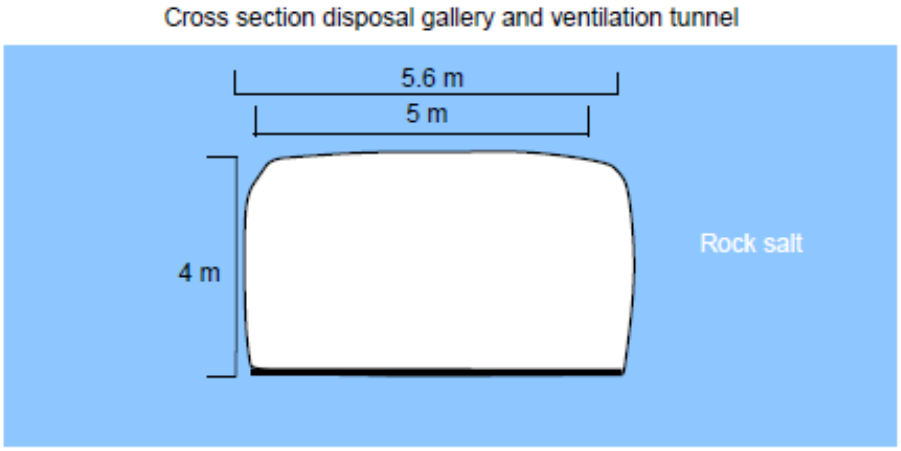

Figure 2-1 Cross sections of the disposal tunnel in the lower level of the repository and the planned arrangement of containers within it. (From COVRA – "Lower_Level_Disposal_Concept.pdf")

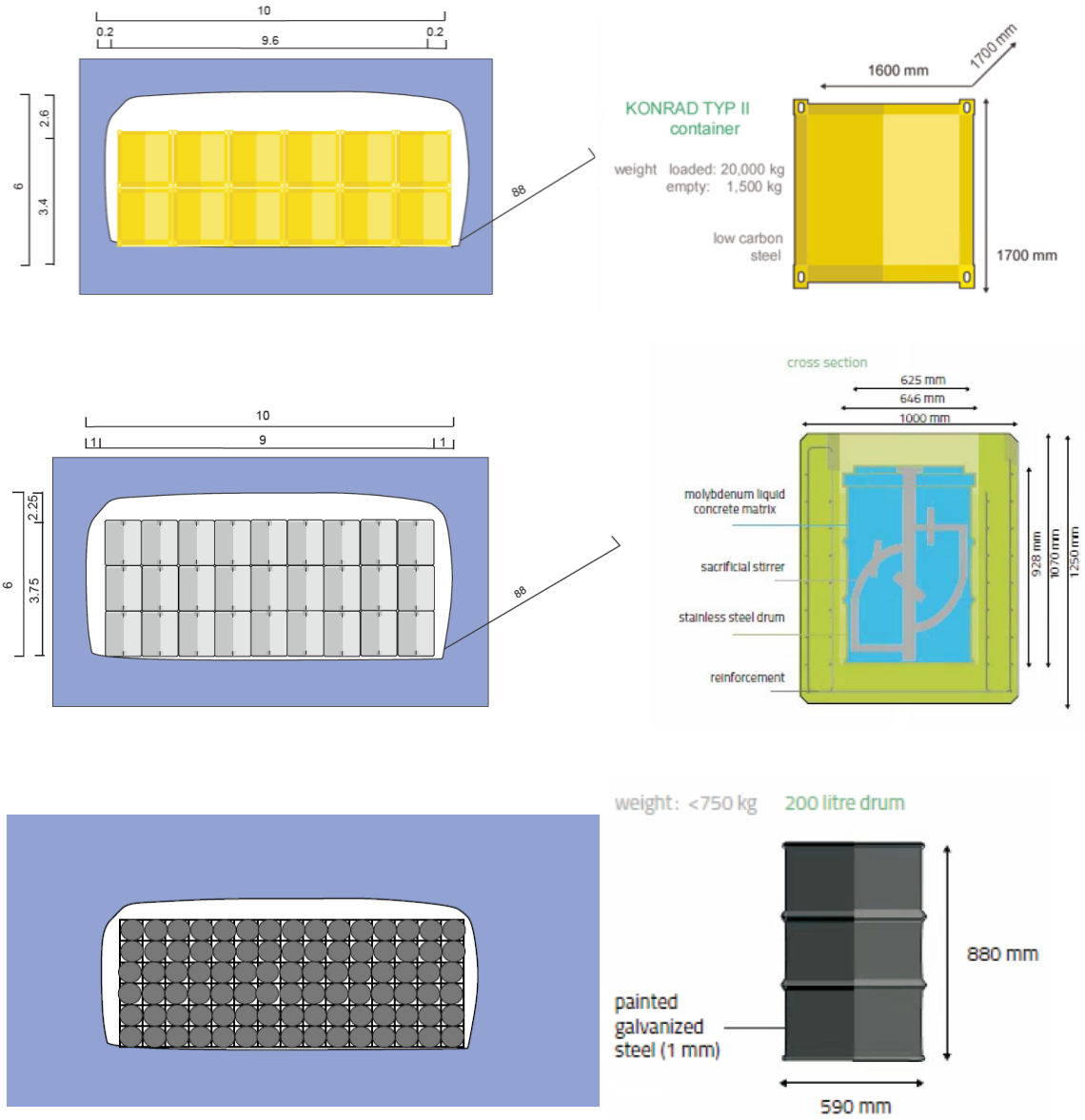

Figure 2-2 Cross sections of the disposal tunnel in the upper level of the repository, and the arrangement of KONRAD containers (top), 1000L containers (middle) and 200L drums (bottom) within it. (From COVRA – "Upper_Level_Disposal_Concept.pdf")

The temperature in and around the package will affect rates of corrosion. The thermal evolution will be determined by the per-package radionuclide inventory, the thermal properties of the package and its surroundings, the inter-package spacing and any co-located wastes, and so is beyond the scope of the current modelling. The model instead allows a time-dependent temperature $T(t)$ (°C) to be imposed, which is applied uniformly to the package (i.e. inside and on the package surface).

COVRA have provided representative thermal profiles for the upper and lower levels of the repository. The fine resolution data provided by COVRA (10 data points per year)

has been coarsened for the purposes of the current modelling. Original and coarsened thermal profiles are shown in Figure 2-3. The coarsened data points are listed in Table 2-1. For simplicity, the temperature at time t=0 y from the profiles (which corresponds to the time that the waste is emplaced in the repository) is also used as the constant temperature while the waste is in storage. This will be higher than the constant ambient temperature in the storage facilities, but corrosion in storage is only assumed to occur within the package where the temperature will be higher than the external ambient temperature, so the approximation may not be overly pessimistic.

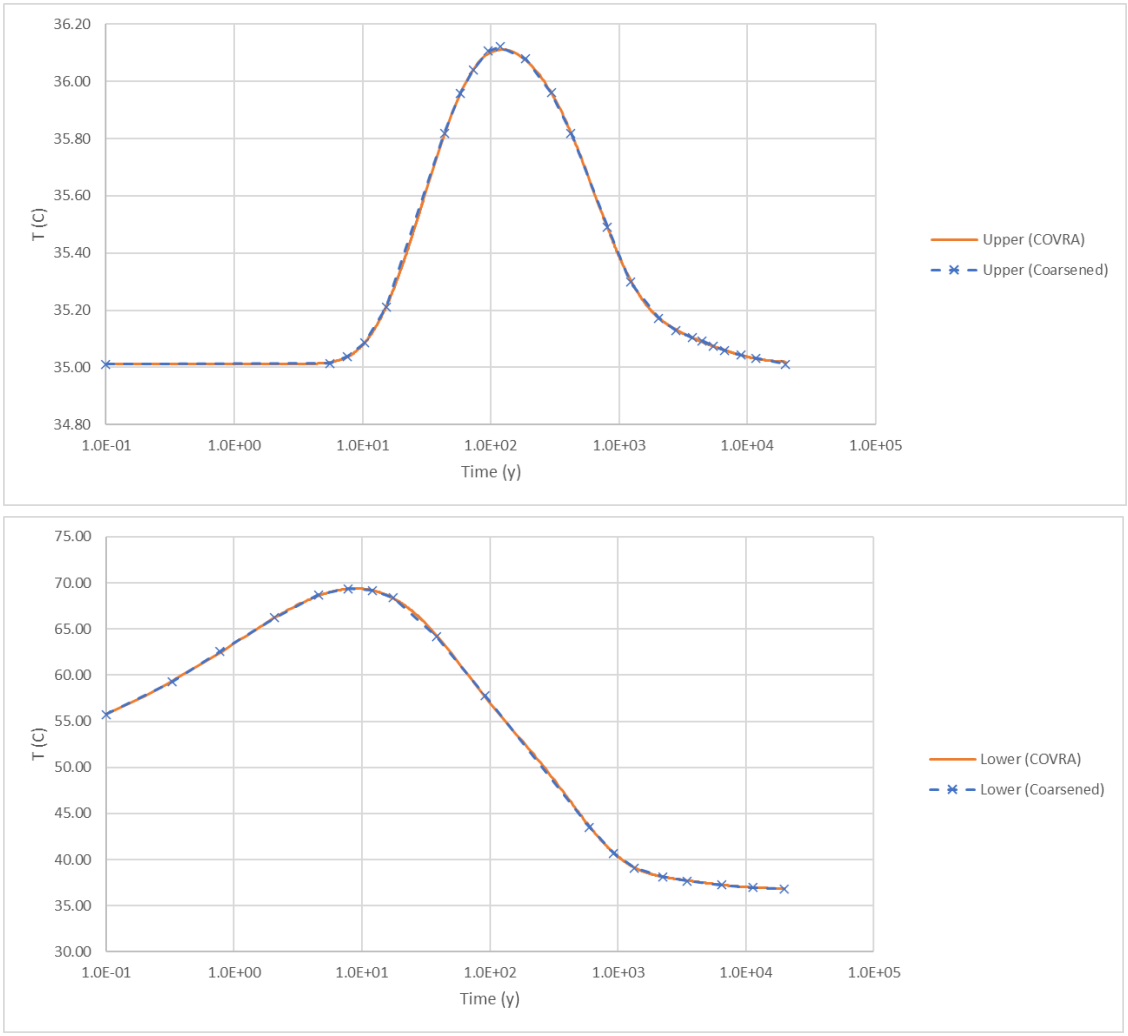

Figure 2-3 Temperature profiles in the upper (top) and lower (bottom) levels of the repository (orange curves) based in Smit (2022) and coarsened data used in the current modelling (blue dashed line/crosses). Time units are time after emplacement in the repository.

Table 2-1 Coarsened temperature profiles used in the current modelling.

Upper Level		Lower Level	
Time (y)	Temperature (°C)	Time (y)	Temperature (°C)
0.10	35.01	0.10	55.72
5.58	35.01	0.33	59.24
7.64	35.04	0.77	62.56
10.37	35.09	2.08	66.21
15.34	35.21	4.59	68.70
43.56	35.82	7.78	69.36
57.54	35.96	12.08	69.20
72.79	36.04	17.57	68.37
95.37	36.11	38.01	64.22
118.61	36.12	91.83	57.75
186.78	36.08	598.33	43.49
296.85	35.96	923.08	40.67
421.24	35.82	1,352.48	39.07
812.25	35.49	2,244.80	38.13
1,225.62	35.30	3,487.35	37.68
2,034.84	35.17	6,461.40	37.24
2,762.53	35.13	11,455.60	36.97
3,750.04	35.10	20,000.00	36.83
4,465.50	35.09		
5,411.32	35.08		
6,614.85	35.06		
8,978.96	35.04		
11,667.11	35.03		
20,000.00	35.01		

A summary of the quantities that are required to define each scenario is given in Table 2-2. Central analysis case values for the scenario-defining quantities for each waste stream are given in Table 2-3, with the exception of the flag determining whether the solid represented by the volume adjacent to the package is cementitious. This is given later in Table 3-6. For all waste groups considered, it has only been possible to obtain radionuclide inventory information at 2130 (Section 3.3.2). For this reason, 2130 has been chosen in the modelling as the time at which all waste group packages are emplaced in the repository, and gas generation due to radiolysis is ignored before this time. A notional 100 y storage period has been selected for all waste groups (equivalent to placing in storage in 2030), so that default values of $t_s = 0$ y and $t_r = 100$ y have been chosen in the modelling.

Table 2-2 Summary of quantities specified in the scenario model. Central analysis case values for each waste group are given in Table 2-3, unless otherwise noted.

Quantity	Units	Description
Operational phase		
t_s	y	Time that the package is placed in storage.
Post-closure phase		
t_r	y	Time that the package is placed in the repository.
$V_{out}^{P}(t)$	m^3	Pore volume adjacent to the waste package, which can vary due to salt creep.
S_{out}^{W}	-	Initial water saturation in the pore volume V_{out}^{P} at time t_r.
$\mathbf{M}_{\mathbf{surround}}$	kg	Mass of solid in which pore volume V_{out}^{P} is assumed to reside.
$Q_{geo}(t)$	kg/y	Rate at which water approaches the waste package from the geosphere (after consideration of any overpack interactions).
$f_{pkg,init}$	-	Initial fraction of water approaching that enters the waste package.
$t_{pkg,fail}$	y	Time at which mechanical failure of the package is assumed (if any).
$f_{pkg,fail}$	-	Fraction of water approaching that enters the waste package after mechanical failure.
Cement surround	-	Flag indicating whether package is encapsulated/emplaced in a cement overpack/container. (See Table 3-6)
$T(t)$	°C	Temperature, assumed to apply uniformly to the package (i.e. inside and on the package surface).

Table 2-3 Central analysis case values for scenario-defining quantities for each waste stream. Q_{geo} is determined by dividing the imposed flow rate per unit tunnel length (kg/m/day) by the number of packages per metre.

	t_s (y)	t_r (y)	$V^P_{out}(t)$ (m^3)	$S^W_{out}(t_r)$ (-)	$M_{surround}$ (kg)	Packages per metre (m^{-1})	$f_{pkg,init}$ (-)	$t_{pkg,fail}$ (y)	$f_{pkg,fail}$ (-)	$T(t)$ (°C)
Vitrified Waste	0	100	10.83	0.1	48,358.40	0.60	0.0	-	-	Table 2-1, lower level
Research Reactor Spent Fuel	0	100	32.48	0.1	145,075.21	0.20	0.0	-	-	Table 2-1, lower level
Uranium Collection Filters	0	100	32.48	0.1	145,075.21	0.20	0.0	-	-	Table 2-1, lower level
Reprocessing Waste	0	100	10.83	0.1	48,358.40	0.60	0.0	-	-	Table 2-1, lower level
HLW Technical Waste (OPERA)**	0	100	32.48	0.1	145,075.21	0.20	0.0	-	-	Table 2-1, lower level
Decommissioning Waste (Revised OPERA HLW Technical Waste)**	0	100	1.26	0*	5,645.15	7.33	1.0*	-	-	Table 2-1, upper level
Legacy Waste (Revised OPERA HLW Technical Waste)**	0	100	2.04	0.1	9,092.15	9.33	0.1	-	-	Table 2-1, upper level
Depleted Uranium	0	100	1.26	0*	5,645.15	7.33	1.0*	-	-	Table 2-1, upper level
Molybdenum Waste	0	100	0.43	0.1	1,902.90	26.40	0.1	-	-	Table 2-1, upper level
Non-Compactible LILW	0	100	0.43	0.1	1,902.90	26.40	0.1	-	-	Table 2-1, upper level
Compactible LILW	0	100	0.12	0.1	529.77	100.00	0.1	-	-	Table 2-1, upper level

(*) The KONRAD container is not included in the analysis. All water from the geosphere is therefore directly available to the package contents as soon as the package is placed in the repository in these cases. The initial water saturation outside of the package in these cases is set to zero to prevent immediate availability of the surrounding water to the package contents.

(**) The HLW Technical Waste group is based on the original specification in OPERA. COVRA are now planning to separate these into two separate waste groups corresponding to decommissioning (in KONRAD packages) and legacy waste (in DDS packages). See Watson (2023).

3 Package-Scale Gas Generation Model

The primary gas generation process that are expected to occur within the waste packages are (Watson, 2023):

- Corrosion,
- Microbial degradation of organic materials, and
- Radiolysis of water and organic materials.

Other processes that could affect the rate of gas generation such as dissolution/exsolution of gas and methanogenesis are outside the scope of this study (Watson, 2023).

The degree to which each process occurs will depend on the availability of the source material and, in most cases, availability of water from the geosphere after closure. Source materials include:

- Metals inside the package (stainless steel, carbon steel, Zircaloy, uranium and aluminium) and exterior waste packaging[1] (stainless steel, galvanised steel and low carbon steel) that can be accessed by water outside the package,
- Organic materials that are subject to microbial degradation, and
- Organic materials that are susceptible to radiolysis.

The current models only consider waste and storage packaging. Overpacks, structures associated with waste emplacement (e.g. stillages) and structural materials and equipment left in the disposal vaults and tunnels are outside the scope of this study (Watson, 2023).

The water composition will affect rates of gas generation. During storage, any water that is present in the waste will initially be oxic and low salinity, although in sealed packages anoxic conditions will quickly develop. Any such water that is not consumed during storage will continue to react after emplacement and closure. Water entering the repository from the host rock will be expected to be anoxic and be of higher salinity (brine). Any brine that contacts waste packages that are emplaced in cementitious overpacks is expected to be alkaline conditioned. Similarly, any brine entering waste packages that are concrete lined or where the waste is encapsulated in a cementitious matrix are also expected to be rapidly alkaline conditioned.

The model solves for the following quantities:

- The remaining amount of metal j at time t, $M_j(t)$ (mol),
- The amount of water in location k at time t, $W_k(t)$ (mol),

[1] For the purposes of the model, packaging metals such as guide rails and rebars are treated as being part of the metal inventory inside the model, and not part of the exterior packaging.

- The amount of organics of type l at time t, $O_l(t)$, and
- The cumulative amount of gas of type i produced at time t, $G_i(t)$ (mol).

In the above, the index j on metals denotes (metal, usage, geometry) combinations. For example a given index j might correspond to 'stainless steel of plate type used for waste packaging' or 'stainless steel of plate type in the waste' (but not both). Water locations k are either inside or outside the package and are denoted with suffices "in" and "out".

3.1 Metal Corrosion Processes

Metal corrosion potentially affects all waste groups in the study. All waste groups include metal packaging and some waste groups have metal waste components or other metal features inside the package, such as rebars or paddles.

Rates of metal corrosion are simulated in the model using a similar approach to that adopted in the SMOGG code (Swift, 2016). The approach adopted in SMOGG is first presented, and then the simplifications assumed in the present model are stated.

Corrosion is generally assumed to be associated with a long-term 'chronic' rate, but periods of rapid 'acute' corrosion can arise when packages are disturbed, e.g. when protective films that may have developed on the metal surfaces are disturbed when waste packages are handled and emplaced. The two modes of corrosion (chronic and acute) have associated timescales so that the overall rate of corrosion of metal j, $F_{corr,j}$ (mol m^{-2} y^{-1}), can be expressed as

$$F_{corr,j}(t) = k_{a,j}e^{-(t-t_d)/t_{a,j}} + k_{c,j}e^{-(t-t_d)/t_{c,j}}. \tag{3.1}$$

Here, $k_{a,j}$ and $k_{c,j}$ (mol m^{-2} y^{-1}) are the corrosion rates associated with the acute and chronic modes of corrosion of metal j respectively, with the rates being molar rates of consumption of the corresponding metal, i.e. moles of Fe in the case of steel components. $t_{a,j}$ and $t_{c,j}$ (y) are associated characteristic timescales of corrosion, which are used to represent the development of passivating films that inhibit corrosion. In (3.1), t_d (y) is the time of the most recent event that disturbed the package – i.e. disturbance events act to reset both the acute and chronic corrosion processes.

If it is assumed that the only disturbance events that occur are the initial handling for placement in storage and the handling for final emplacement in the repository, then if t_s (y) is the time that the package is placed in storage and t_r (y) is the time that it is placed in the repository relative to a time origin, such as present day, (from the storage and disposal scenario model – Section 2), the corrosion rate can then be written

$$F_{corr,j}(t) = \begin{cases} 0 & t < t_s, \\ k_{a,j}e^{-(t-t_s)/t_{a,j}} + k_{c,j}e^{-(t-t_s)/t_{c,j}} + k_{e,j} & t_s \le t < t_r, \\ k_{a,j}e^{-(t-t_r)/t_{a,j}} + k_{c,j}e^{-(t-t_r)/t_{c,j}} + k_{e,j} & t_r \le t. \end{cases} \tag{3.2}$$

In (3.2), an additional rate $k_{e,j}$ (mol m^{-2} y^{-1}) has been added to allow simple cases with no assumed development of passivating layers to be represented, e.g. where no suitable timescale data is available. It is expected that either $k_{a,j}$ and $k_{c,j}$ are specified and $k_{e,j} = 0$, or $k_{a,j}, k_{c,j} = 0$ and $k_{e,j}$ is specified.

The corrosion rates $k_{a,j}$, $k_{c,j}$ and/or $k_{e,j}$ are specific to each type of metal (waste metals include stainless steel, carbon steel, Zircaloy, uranium, Magnox and aluminium and waste packaging includes stainless steel, galvanised steel and low carbon steel). Additionally, they typically only apply when water is present and vary with chemical conditions (oxic/anoxic, neutral/alkaline, low/high chloride). They can also vary with temperature (which can be a function of time).

To implement the full SMOGG-style model, corrosion rates must be provided for all metals for all combinations of porewater conditions that can arise in the scenarios to be simulated, with values given as a function of temperature. Up to eight different porewater conditions can arise, one for each combination of oxic/anoxic, low/high chloride, neutral/alkaline conditions that can occur in the disposal scenario. The subscripts ox/anox, lowCl/highCl and neut/alk are used to distinguish the rates so that, for example, $k_{a,j,anox,highCl,alk}$ denotes the acute rate for metal j under anoxic, high chloride, alkaline conditions.

Most corrosion reactions require water to be present, and therefore only apply when the metal (either inside the package or on the outer package surface) is in contact with water. Presence of water inside and outside the package is denoted by (smoothed) unit step functions $s_k(t)$ (-) indicating the presence ($s_k = 1$) or absence ($s_k = 0$) of water in location k. Metal indices j corresponding to metals used for exterior packaging materials will have "in" and "out" reaction rates that are both non-zero, since these can potentially be corroded simultaneously from the inside and outside.

With $f_{anox}(t)$, $f_{highCl}(t)$ and $f_{alk}(t)$ denoting the timing functions for anoxic, high chloride and alkaline conditions from the storage and disposal scenario model, which are 1 when the corresponding condition occurs and zero otherwise, the corrosion rate terms at any time can be calculated as

$$k_{x,j,k}(t) = \sum_{u\in\{ox,anox\}} \sum_{v\in\{lowCl,highCl\}} \sum_{w\in\{neut,alk\}} f_{u,k} f_{v,k} f_{w,k} k_{x,j,u,v,w}\, s_k(t), \quad \text{for } x \in \{a, c, e\}, \tag{3.3}$$

where $f_{ox}(t) = 1 - f_{anox}(t)$, $f_{lowCl}(t) = 1 - f_{highCl}(t)$ and $f_{neut}(t) = 1 - f_{alk}(t)$. The reason for the index k on the corrosion rate and on the timing functions, which represents the location (inside or outside the package) is explained below. Generally, only one term in the summation will be non-zero, except at transition times between periods of different chemical conditions where two or more terms may be present during any 'smoothing period' over which the switching of the conditions occurs.

The corrosion rate terms in equation (3.3) must be calculated separately for the interior and the exterior of the package because the porewater conditions can potentially be different inside and outside of the package. For example, if the waste includes a cement matrix then it would be assumed that $f_{alk,in} \equiv 1$ inside the waste package regardless of the alkalinity of the water approaching the outside of the package. The $F_{corr,j}$ terms therefore require an additional indexing k to denote the location of the water that is reacting, which was omitted in (3.2) for simplicity and for consistency with the notation in Appendix A, where reaction rate parameters are given for each metal. $F_{corr,j,k}$ should be taken to refer to the corrosion rate of metal j due to water in location k, which can therefore distinguish the corrosion of 'stainless steel of plate type used for waste packaging' (metal j) from water inside (k="in") and outside (k="out") the package. Waste (non-exterior packaging) metals will only have a k="in" contribution.

To simplify the current model, it will be assumed that:

- Corrosion of all metals can be represented assuming no development of passivating layers, so that a constant rate $k_{e,j}$ applies for all metals.
- In storage, there is no corrosion of the exterior of the packaging.
- In the repository, any porewater corroding the exterior of the package is:
    - always alkaline if the package is surrounded by cement and always neutral otherwise.
    - always anoxic and high chloride.
- For open/vented packages:
    - In storage, any porewater corroding the contents and inner surface of the waste package is:
        - always alkaline if the waste package contains cement and always neutral otherwise.
        - always oxic and low chloride.
    - In the repository, any porewater corroding the contents and inner surface of the waste package is:
        - always alkaline if the waste package contains cement or if the package is surrounded by cement and always neutral otherwise.
        - always anoxic and high chloride.
- For sealed packages:
    - In storage, or until the time of corrosive or mechanical failure of the packaging in the repository, any porewater in the waste package that corrodes its contents and inner surface is:
        - always alkaline if the waste package contains cement and always neutral otherwise.
        - always anoxic, since any initially oxic conditions will relatively quickly become anoxic as water is consumed.
        - always low chloride.

    - In the repository, and after the time of failure of the packaging, any porewater corroding the contents and inner surface of the waste package is:
        - always alkaline if the waste package contains cement or if the package is surrounded by cement and always neutral otherwise
        - always anoxic and high chloride.
- All metals in the waste (not packaging) of the same type are treated collectively as a bulk metal. E.g. stainless steel filter housings and stainless steel filters in the uranium collection filters waste group are treated as a single stainless steel inventory. The reactive surface area (see below) for the bulk metal is calculated as a mass-weighted average of the reactive surface areas of each metal.
    - This is only a simplification in terms of the parameterisation of the model. Additional metal species can be easily introduced to the model if it is found necessary to distinguish gas generation from different instances of the same type of metal.

Note that it is implicitly assumed that there is no transient period whereby, for example, oxic water remaining in the waste from storage gradually becomes anoxic after the package is placed in the repository. Any such changes are assumed to happen instantly.

The first assumption, that the development of passivating layers can be ignored so that the corrosion rate can be represented by a constant rate $k_{e,j}$ requires some justification. The corrosion rates for the metals considered are given in Appendix A. The only metals for which an acute corrosion rate is available are galvanised steel (which is simulated as mild steel, i.e. any benefit of galvanisation on gas generation is neglected), zircaloy and aluminium. Figure 3-1 shows the cumulative integral of $r(t) = F_{corr,j}/F_{chronic,j}$, where $F_{chronic,j}$ (mol m^{-2} y^{-1}) is equal to $F_{corr,j}$ with the acute part omitted. If the acute part of $F_{corr,j}$ was zero, then $r(t) = 1$ would result and so the cumulative integral would be expected to be linear. Any deviation from linear behaviour reflects the effect of the acute corrosion term. The plot shows that for timescales on the order of 100 y the effect of the acute phase of corrosion on the total generated gas will be small, and probably negligible in the context of other uncertainties in the model. For example, a simulation with chronic corrosion rates increased by 10% would easily bound the additional effect of the acute rate over timescales of 100 y. The acute phase of corrosion would only be expected to make a significant difference in the long-term if there were repeated disturbances to the canister, resulting in repeated periods of acute corrosion.

Regarding the choice of constant corrosion rates $k_{e,j}$, the chronic corrosion rates found for each metal (Appendix A) all have associated chronic corrosion timescales that are effectively infinite (they are stated to be 10^8 y in all cases). Therefore, the chronic components of the identified corrosion rates are effectively all constant and so the

constant corrosion rate $k_{e,j}$ will be taken to be equal to the identified chronic corrosion rate. With this simplifying assumption, (3.2) reduces to

$$F_{corr,j}(t) = \begin{cases} 0 & t < t_s \\ k_{c,j} & t_s \leq t. \end{cases} \quad (3.4)$$

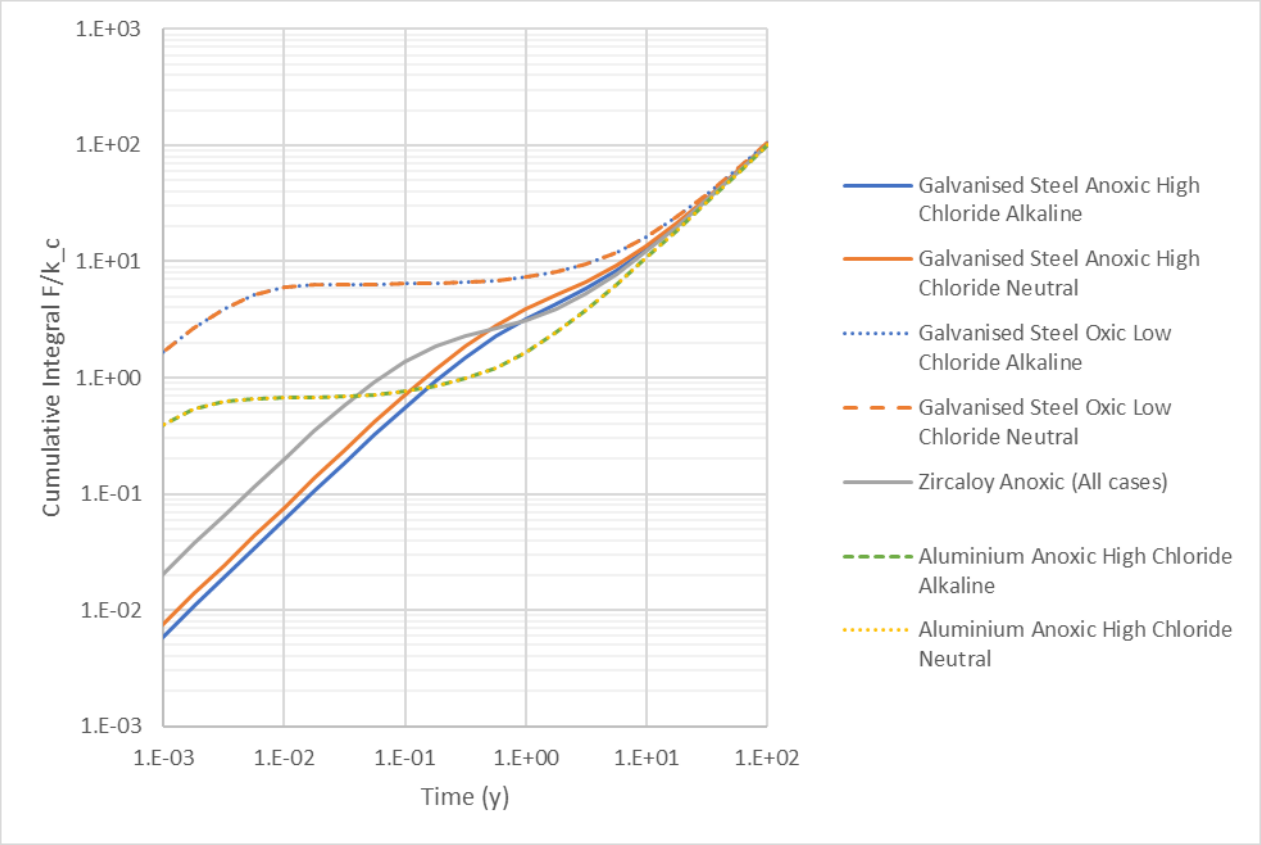

Figure 3-1 Cumulative integral of $F_{corr,j}/F_{chronic,j}$ for metals where both acute and chronic corrosion rate data is available (Appendix A). The long-term trend is linear, with a gradient 1, meaning that the effect of any acute phase of corrosion is quickly diminished over timescales of ~100 y.

The other simplifying assumptions correspond to specific choices of the timing functions $f_{u,k}$, $f_{v,k}$ and $f_{w,k}$ in (3.3), which set the functions identically to 1 or 0 depending on the disposal scenario and time. With the simplifying assumptions, for open/vented packages (3.2)-(3.3) reduce to

$$F_{corr,j,out}^{OPEN}(t) = \begin{cases} 0 & t < t_s, \\ 0 & t_s \le t < t_r, \\ \begin{cases} k_{e,j,anox,highCl,alk} \\ k_{e,j,anox,highCl,neut} \end{cases} & \begin{matrix} \text{if surrounded by cement} \\ \text{otherwise} \end{matrix} \quad t_r \le t. \end{cases},$$

$$F_{corr,j,in}^{OPEN}(t) = \begin{cases} 0 & t < t_s, \\ \begin{cases} k_{e,j,ox,lowCl,alk} \\ k_{e,j,ox,lowCl,neut} \end{cases} & \begin{matrix} \text{if cementitious} \\ \text{otherwise} \end{matrix} \quad t_s \le t < t_r, \\ \begin{cases} k_{e,j,anox,highCl,alk} \\ k_{e,j,anox,highCl,neut} \end{cases} & \begin{matrix} \text{if cementitious, or if} \\ \text{surrounded by cement} \\ \text{otherwise} \end{matrix} \quad t_r \le t. \end{cases}. \tag{3.5}$$

For sealed packages, the corresponding simplification is

$$F_{corr,j,out}^{SEALED}(t) = \begin{cases} 0 & t < t_s, \\ 0 & t_s \le t < t_r, \\ \begin{cases} k_{e,j,anox,highCl,alk} \\ k_{e,j,anox,highCl,neut} \end{cases} & \begin{matrix} \text{if surrounded by cement} \\ \text{otherwise} \end{matrix} \quad t_r \le t. \end{cases},$$

$$F_{corr,j,in}^{SEALED}(t) =$$

$$\begin{cases} 0 & t < t_s \\ \begin{cases} k_{e,j,anox,lowCl,alk} \\ k_{e,j,anox,lowCl,neut} \end{cases} & \begin{matrix} \text{if cementitious} \\ \text{otherwise} \end{matrix} \quad t < t_{pkg,fail} \text{ and } f_{pkg,corrode} < 1 \\ \begin{cases} k_{e,j,anox,highCl,alk} \\ k_{e,j,anox,highCl,neut} \end{cases} & \begin{matrix} \text{if cementitious, or if} \\ \text{surrounded by cement} \\ \text{otherwise} \end{matrix} \quad t_{pkg,fail} \le t \text{ or } f_{pkg,corrode} = 1 \end{cases} \tag{3.6}$$

In the above, $f_{pkg,corrode}$ (-) is the degree to which the packaging is corroded and is discussed below. All rates are additionally scaled by the water scaling function $s_k(t)$ described above so that reactions only occur in the presence of water.

The main differences between the reaction rates for the open/vented and sealed packages are that:

- The 'trigger' for changing the mode of corrosion of the interior of the package is emplacement in the repository in the case of open/vented packages and is mechanical or corrosive failure in the case of sealed packages.
- Porewater conditions prior to the 'trigger' are oxic for open/vented packages and anoxic for sealed packages.

After the simplifications, up to three reaction rates are required for each metal depending on whether the metal experiences alkaline and/or neutral conditions in the storage and packaging scenarios that are considered. For example, a metal in a non-cementitious waste form that does not encounter water during storage and that is not emplaced in a cement overpack would only require $k_{e,j,\text{anox,highCl,neut}}$ to be specified. A waste metal in a cementitious waste form in an open/vented package that can corrode in storage in addition to corroding after disposal would require $k_{e,j,\text{ox,lowCl,alk}}$ (corrosion

inside during storage) and $k_{e,j,\text{anox,highCl,alk}}$ (corrosion inside after emplacement) to be specified. A packaging metal in an open/vented package for cement-encapsulated waste that corrodes internally in storage and that is not emplaced in cement would require $k_{e,j,\text{ox,lowCl,alk}}$ (corrosion inside during storage), $k_{e,j,\text{anox,highCl,alk}}$ (corrosion inside after emplacement) and $k_{e,j,\text{anox,highCl,neut}}$ (corrosion outside after emplacement) to be specified.

Parameter values to be used in the modelling are given in Appendix A, which also provide the stoichiometries of gas (hydrogen) produced in the corrosion reactions. The tables identify the porewater condition combinations that are screened out as a consequence of the simplifying assumptions that are made.

The above corrosion rates apply over a reactive surface area, $A_{j,k}(t)$ (m^2), that depends on the geometry of the metal features and the location. In the first instance, all metal areas will be determined assuming a plate geometry with a specified thickness. This is conservative in the sense that the surface area will not shrink, as it would for a cylindrical geometry, and so will maximise the gas generation rate. If the model is updated to include alternative metal geometries in future then, if the same metal is present in different geometrical forms (e.g. plates and cylinders) in the waste, then these would need to be treated separately in the model since the surface area term $A_{j,k}$ would need to be calculated differently for the different metal geometries. A different index j would be used for each case.

The choice to treat metals in the waste that are of the same type collectively as a bulk metal does not affect the net amount of gas that can be produced, but can affect the time scale over which it is produced. The contribution to the averaging of the reactive surface area from components with larger reactive surface areas will tend to accelerate reactions for metals with smaller surface areas and vice versa. The net effect will generally be to accelerate the overall rate of reaction for the metal, causing it to be depleted earlier in the evolution, and so should be a conservative choice.

The one-sided geometric area, e.g. A = length×width, is specified for metals with plate geometry. For non-packaging metals inside the waste, the effective surface area for corrosion computed by the model will be $2A$, since both sides of the metal will be available for corrosion. For packaging metals, only one side of the metal is presented to the water inside and outside of the package and therefore the effective surface area in each location is A, but the total reactive surface area will only be $2A$ if water is present both inside and outside the package.

The rate of consumption of metal with index j, $R_{corr,j}$ (mol/y), is therefore

$$R_{corr,j}(t) = (A_{j,in}(t)F_{corr,j,in}(t) + A_{j,out}(t)F_{corr,j,out}(t))H\left(M_j(t)\right), \qquad (3.7)$$

The Heaviside function of the remaining amount of metal is present to halt the reaction when the metal j is fully corroded.

Given the molar volume, $V_{M,j}$ (m^3/mol) of metal j, the rate of change of the depth of corrosion of metal with index j, l_j (m), is given by

$$\frac{dl_j}{dt} = \left(V_{M,j}F_{corr,j,out}(t) + V_{M,j}F_{corr,j,in}(t)\right) H\left(M_j(t)\right). \quad (3.8)$$

The depth of corrosion is monitored in the model to determine the timing of corrosive failure of the external waste packaging, at which time it is assumed that all water that would have contributed to corrosion of the exterior of the waste package is then available for corrosion in the interior of the package. The fraction corroded, $f_{pkg,corrode}$ (-), is determined by

$$f_{pkg,corrode} = 1 - \frac{M_{j^*}(t)}{M_{j^*}(0)}, \quad (3.9)$$

where j^* is the index of the metal representing the outer packaging. The outer packaging is required to be 99% corroded in order for the package to be corrosively failed. This occurs when $f_{\mathrm{pkg,corrode}}$ reaches 0.99, at which point water approaching from the geosphere is assumed to enter the package (unless it is already saturated). The rate at which water enters the package then ramps up to the full geosphere rate once the package becomes fully corroded. This definition of corrosive failure in terms of the fraction corroded is extreme. In reality it would be expected that the package will fail to protect against ingress of water as soon as it is corroded at its thinnest point. Such uncertainties can be explored in the model in various ways, such as imposing a mechanical failure time or reducing the amount of packaging metal and reassigning the remainder of the metal to the interior of the package.

At the time of corrosive failure any water remaining in the pore space outside the package is transferred to the interior of the package using a fast kinetic rate, subject to availability of open (non-water-filled) pore and/or void space to accommodate the water (Section 3.4). This choice leads to maximal corrosion / gas generation. To analyse sensitivity to the assumption that the packaging metal must fully corrode before the interior of a closed package is exposed to water, the $t_{pkg,fail}$ and $f_{pkg,fail}$ parameters (Section 2) can be used to impose earlier package failure than that associated with complete corrosion. In this case, the packaging will continue to corrode from both sides until fully corroded.

The stoichiometry of water consumed in the corrosion reaction and the stoichiometry of gas produced can vary with the porewater conditions (if a different corrosion reaction occurs under different conditions). The stoichiometry of water in location k in the corrosion reaction for metal j, $\mathcal{S}^w_{j,k}$ (-) is calculated generally as

$$\mathcal{S}^{W}_{j,k}(t) = \sum_{u\in\{ox,anox\}} \sum_{v\in\{lowCl,highCl\}} \sum_{w\in\{neut,alk\}} f_u f_v f_{w,k} \mathcal{S}^{W}_{j,u,v,w}\,, \tag{3.10}$$

where $\mathcal{S}^{W}_{j,u,v,w}$ (-) is the stoichiometry of water in the corrosion reaction for the combination of porewater conditions (u, v, w). With the simplifying assumptions, this becomes

$$\mathcal{S}^{W}_{j,out}(t) = \begin{cases} 0 & t < t_s, \\ 0 & t_s \le t < t_r, \\ \begin{cases} \mathcal{S}^{W}_{j,anox,highCl,alk} \\ \mathcal{S}^{W}_{j,anox,highCl,neut} \end{cases} & \text{if surrounded by cement} \\ & \text{otherwise} \end{cases} \quad t_r \le t. \end{cases},$$

$$\mathcal{S}^{W}_{j,in}(t) = \begin{cases} 0 & t < t_s, \\ \begin{cases} \mathcal{S}^{W}_{j,ox,lowCl,alk} \\ \mathcal{S}^{W}_{j,ox,lowCl,neut} \end{cases} & \text{if cementitious} \\ & \text{otherwise} \end{cases} \quad t_s \le t < t_r, \\ \begin{cases} \mathcal{S}^{W}_{j,anox,highCl,alk} \\ \mathcal{S}^{W}_{j,anox,highCl,neut} \end{cases} & \text{if cementitious, or} \\ & \text{if surrounded by cement} \\ & \text{otherwise} \end{cases} \quad t_r \le t. \end{cases}, \tag{3.11}$$

Similarly, the stoichiometry of gas i in the corrosion reaction for metal j, $\mathcal{S}^{G}_{i,j,k}$ (-) is calculated as

$$\mathcal{S}^{G}_{i,j,k}(t) = \sum_{u\in\{ox,anox\}} \sum_{v\in\{lowCl,highCl\}} \sum_{w\in\{neut,alk\}} f_u f_v f_{w,k} \mathcal{S}^{G}_{i,j,u,v,w}, \tag{3.12}$$

which has simplified form analogous to (3.11).

The rate of consumption of water in location k due to corrosion of all metals accessible from location k, $Q_{corr,k}$ (mol/y) is then

$$Q_{corr,k} = \sum_{j} \mathcal{S}^{W}_{j,k}(t) A_{j,k}(t) F_{corr,j,k}(t) s_k(t), \tag{3.13}$$

and rate of production of gas i due to corrosion of all metals, $P_{corr,i}$ (mol/y), is

$$P_{corr,i} = \sum_{j} \sum_{k} \mathcal{S}^{G}_{i,j,k}(t) A_{j,k}(t) F_{corr,j,k}\,(t)\, s_k(t). \tag{3.14}$$

Amounts of each metal of each type of geometry used in packaging and occurring in the waste are given in Table 3-1 for each waste group.

3.1.1 Metal Inventory by Waste Group

The metal inventories per waste group are given in the following tables. In each case, references to the original data sources are provided. Where masses of metals per container have been provided in the OPERA documentation, these are used directly to calculate the molar amounts of each metal. Where the metal type or steel composition has not been specified, an assumption has been made by analogy with other waste groups or using knowledge about the waste stream. For some waste groups, the amounts of each metal have been estimated using the dimensions of each component. The notes columns in the following tables detail how the metal amounts and surface areas were derived for each waste group.

In the case of HLW Technical Waste, two approaches are taken. In the first, the inventory is calculated for the ECN packaging given in OPERA. The second approach reflects COVRA's revised plan to separate the original HLW Technical Waste into decommissioning waste (in KONRAD packages) and legacy waste (in DDS packages). Only the revised waste groups are considered in the modelling in Benbow et al. (2023).

Table 3-1 Amounts of each metal (moles of metal element indicated) of each type of geometry used in packaging and occurring in the waste for each waste group. A plate geometry is assumed for all metals. One-sided areas, A_j (m²), are given.

Vitrified Waste

Location	Metal	Metal amount M_j (mol)	Area A_j (m²)	Notes	Source/Reference
Outer Packaging (CSD-v Container)	Stainless Steel	80 kg steel -> 55.911 g/mol -> 1.5E+03 mol stainless steel	2.1E+00	Outer surface area approximated assuming simplified cylindrical geometry (1335 mm height, 430 mm outer diameter). Moles of stainless steel calculated from steel mass (80 kg) and molar mass of stainless steel (55.911 g/mol).	Dimensions from Fig 3-1 in Verhoef et al. (2016) and steel type ("as per NF EN 10095") in text below. Mass from Table 3-8 in Meeussen and Rosca-Bocancea (2014).

Research Reactor Spent Fuel

Location	Metal	Metal amount M_j (mol)	Area A_j (m^2)	Notes	Reference
Outer Packaging (ECN Canister)	Stainless Steel	105 kg steel -> 55.911 g/mol -> 1.9E+03 mol stainless steel	3.9E+00	Outer surface area approximated assuming simplified cylindrical geometry (846 mm diameter lid, 730 mm diameter base, area of sides calculated assuming 740 mm diameter and 1236 mm height). Moles of stainless steel calculated from steel mass (105 kg) and molar mass of stainless steel.	Dimensions and steel type (304L) from Fig 3-2 in Verhoef et al. (2016). Mass from text of Section 3.2 in Meeussen and Rosca-Bocancea (2014).
Package Contents (Borated Steel Basket)	Stainless Steel	530 kg steel -> 55.911 g/mol -> 9.7E+03 mol stainless steel	1.2E+01	Total surface area, estimated (cylinder with diameter 740 mm and height 924 mm, with 33 cuboid holes of 81x77x924mm). Moles of steel calculated from steel mass (530 kg) and molar mass of stainless steel.	Dimensions approximated from Fig 3-2 in Verhoef et al. (2016). Mass from text of Section 3.2 in Meeussen and Rosca-Bocancea (2014).
Package Contents (Fuel Capsule)	Aluminium (Al)	5.1E-01 kg Al 26.98 g/mol Al -> 1.9E+01 mol Al	1.9E-01	Outer surface area approximated using simplified cuboidal geometry (81x77x924mm) and 33 per canister. Moles of Al calculated from surface area, thickness (assumed 1 mm), aluminium density (2700 kg/m^3) and molar mass of Al (26.98 g/mol)	Dimensions from Fig 3-2 in Verhoef et al. (2016). Material type and thickness clarified by email 04/10/22.
Package Contents (Fuel Plates & Cladding)	Aluminium (Al)	1.5E+02 kg Al 26.98 g/mol Al -> 5.4E+03 mol Al	2.9E+01	Area and mass calculated per LEU & HEU fuel assembly, then multiplied by 33 fuel assemblies per canister and averaged by 30:120 HEU:LEU proportion of canisters. Cladding surface area (single side of plates) approximated using simplified rectangular geometry: for LEU (HEU), fuel height 600 mm, 18 (21) inner fuel plates with 71.02 mm length & 2 outer with 71.12 mm length. Uranium LEU (HEU) mass given as 550 g (450 g) U-235 in fuel element, 19.75% (93%) enrichment. Uranium-aluminium and uranium-silicon fuel alloys all treated as aluminium for simplification. Aluminium moles calculated from mass of aluminium (70 kg) plus mass of fuel, and molar mass (26.98 g/mol).	Dimensions and mass of fuel from Fig 3-2 and Table 3-3 and other text in Section 3.2.2 of Verhoef et al. (2016). Mass of aluminium from Table 3-7 in Meeussen and Rosca-Bocancea (2014) (used maximum per container). (Calculated mass of uranium compared with this table – close to maximum estimate and within range).

Uranium Collection Filters

Location	Metal	Metal amount M_j (mol)	Area A_j (m^2)	Notes	Reference
Outer Packaging (ECN Canister)	Stainless Steel	105 kg steel -> 55.911 g/mol -> 1.9E+03 mol stainless steel	3.9E+00	Same as RRSF	Verhoef et al., 2016; Meeussen and Rosca-Bocancea, 2014
Package Contents (Aluminium Drum – 5000 series)	Aluminium (Al)	9.3E+01 kg Al 26.98 g/mol Al -> 3.4E+03 mol Al	7.7E+00	Outer surface area approximated using simplified cylindrical geometry (85 mm diameter, 830 mm height). Multiplied by max 33 drums per waste container. Mass of empty aluminium drum provided as 2.82 kg, multiplied by 33 drums, divided by molar mass of aluminium. (Consistent with surface area estimate – implies average drum thickness of 4.5 mm)	Dimensions from Fig 3-5 and text in Section 3.3.2 of Verhoef et al. (2016). Mass of empty drum provided by email 30/08/22.
Package Contents (Filter House)	Stainless Steel	8.5E+02 kg steel -> 55.911 g/mol -> 1.5E+04 mol stainless steel	1.2E+00	Surface area of one side of plate estimated using rectangular geometry (161 mm height, 78.1 mm width). Max 99 filter houses per canister. Volume estimated assuming 85 mm thickness. Moles of stainless steel estimated assuming same steel density (8000 kg/m^3) as spent fuel canister.	Dimensions from Fig 3-5 and text in Section 3.3.2 of Verhoef et al. (2016). Material confirmed as stainless steel by email 30/08/22.
Package Contents (Uranium Collection Filters)	Stainless Steel	5.1E+02 kg steel -> 5.911 g/mol -> 9.2E+03 mol stainless steel	6.3E+02	Volume estimated assuming the filter house volume filled with 60% porosity. Surface area estimated assuming 0.1 mm thickness. Moles of stainless steel estimated assuming same steel density (8000 kg/m^3) as filter house.	Dimensions from Fig 3-5 and text in Section 3.3.2 of Verhoef et al. (2016).

Reprocessing Waste

Location	Metal	Metal amount M_j (mol)	Area A_j (m²)	Notes	Reference
Outer Packaging (CSD-c Container)	Stainless Steel	80 kg steel -> 55.911 g/mol -> 1.5E+03 mol stainless steel	2.1E+00	Same as vitrified	Verhoef et al., 2016; Meeussen and Rosca-Bocancea, 2014
Package Contents (Waste – Compacted Pucks)	Stainless Steel	1.16E+02 kg steel -> 55.911 g/mol -> 2.1E+03 mol stainless steel	2.8E+00	Geometry estimated from PWR fuel assemblies, ends estimated as 200 mm diameter and 200 mm height. From mass (116 kg) and density (assumed 8000 kg/m³), calculated average number per container. Moles of stainless steel calculated from mass (116 kg).	Mass from Table 3-10 of Meeussen and Rosca-Bocancea (2014). Geometry approximated from PWR fuel assembly geometry from: https://www.nuclear-power.com/nuclear-power-plant/nuclear-fuel/.
	Zircaloy (Zr)	3.9E+02 kg Zircaloy -> 98.8% Zr 91.224 g/mol Zr -> 4.3E+03 mol Zr	1.0E+02	Reactive surface area given as ~200 m² per CSD-c assuming both sides of cladding exposed, halved here. Moles of Zr calculated from mass (393 kg), assumed chemical composition (98.8% Zr) and molar mass of Zr (91.224 g/mol).	Reactive surface area from Box 6-2 of Verhoef et al. (2017). Mass from Table 3-10 of Meeussen and Rosca-Bocancea (2014) Zircaloy chemical composition from: https://en.wikipedia.org/wiki/Zirconium_alloy

HLW Technical Waste (OPERA)

Location	Metal	Metal amount M_j (mol)	Area A_j (m²)	Notes	Reference
Outer Packaging (ECN Canister)	Stainless Steel	105 kg steel -> 55.911 g/mol -> 1.9E+03 mol stainless steel	3.9E+00	Same as RRSF	Verhoef et al., 2016; Meeussen and Rosca-Bocancea, 2014
Package Contents (Steel Inner Container and compacted puck packaging)	Stainless Steel	8.4E+01 kg steel -> 55.911 g/mol -> 1.5E+03 mol stainless steel	3.1E+00	Outer surface area calculated as cylinder with radius 330 mm and height 1.156 m. Moles of steel calculated assuming 5 mm thickness (over-estimated to potentially account for compacted puck packaging) and density 8000 kg/m³.	Dimensions estimated from Figure 4-3 of Verhoef et al. (2016)
Package Contents (Waste – Compacted Pucks)	Stainless Steel	10.45 kg steel -> 55.911 g/mol -> 1.9E+02 mol stainless steel	1.0E+02	Assumed area same as reprocessing waste. Moles of steel and aluminium calculated assuming mass of irradiated metal per container (20.9 kg*) is 50% steel and 50% aluminium by mass.	Mass of irradiated metal from Section 4.2.2 of Verhoef et al. (2016)
	Aluminium (Al)	10.45 kg Al -> 26.98 g/mol -> 3.9E+02 mol Al	1.0E+02		

(*) The quoted mass of 20.9 kg of irradiated metal per container appears too small to account for all metal in the waste. It is suspected that there must be additional metal or other materials in the waste form in order to satisfactorily fill the package. It has not been possible to find this information in the OPERA reports. Since the total mass of the waste group is carried forward into the new revised decommissioning and legacy waste forms, those waste forms may also underestimate the amount of metal in the packages.

Legacy Waste (Revised OPERA HLW Technical Waste)

Location	Metal	Metal amount M_j (mol)	Area A_j (m^2)	Notes	Reference
Outer Packaging (DDS Drum)	Stainless Steel	3.8E+1 kg steel -> 55.911 g/mol Fe -> 6.8E+2 mol Fe	6.5E-01	Surface area approximated as two 0.449 m tall cylinders, one with diameter 0.25 m and one with diameter 0.125 m. Moles of steel calculated from approximate volume, assuming wall thickness 4 mm and lid thickness 21 mm, steel density 8000 kg/m^3 and molar mass of stainless steel.	Dimensions, empty mass and material type from technical drawing 47214-22 supplied by email 26/10/22.
Package Contents (Crinkle Barrel)	Stainless Steel	3.8E+1 kg steel -> 55.911 g/mol Fe -> 6.8E+2 mol Fe	6.5E-01	Surface area approximated as two 0.449 m tall cylinders, one with diameter 0.25 m and one with diameter 0.125 m. Moles of steel calculated from approximate volume, assuming wall thickness 4 mm and lid thickness 21 mm, steel density 8000 kg/m^3 and molar mass of stainless steel.	Dimensions from technical drawing 50396-02 supplied by email 26/10/22.
Package Contents (Inserts)	Stainless Steel	2.6E+00 kg steel -> 55.911 g/mol -> 4.6E+1 mol Fe	8.0E-01	Surface area calculated for two half-round and one round insert per container, each with height 0.444 m and radius 0.12495 m. Moles of Fe calculated from empty mass (0.65 kg per half-round, 1.25 kg round) and molar mass of stainless steel.	Dimensions, empty mass and material type from technical drawings 'Halfronde Insert 3 MM rubber 3 MM lood' and 'Ronde insert 3 MM rubber 3 MM lood' supplied by email 26/10/22.
Package Contents (Legacy Waste)	Stainless Steel	1.2E-01 kg steel -> 55.911 g/mol -> 2.1E+00 mol stainless steel	1.5E-02	Mass of irradiated metal per ECN container given as 20.9 kg*, assumed to be 50% stainless steel and 50% aluminium by mass. Redistributed inventory across KONRAD and DDS containers by volume and number of containers (521 KONRAD containers, 0.21 m^3 capacity per container). Surface area estimated assuming 1 mm thick strips, using steel density of 8000 kg/m^3 and aluminium density of 2700 kg/m^3.	Mass of irradiated metal from Section 4.2.2 of Verhoef et al. (2016). Number of KONRAD and DDS containers supplied by email 25/11/22.
	Aluminium (Al)	1.2E-1 kg Al 26.98 g/mol Al -> 4.3E+0 mol Al	4.3E-02		

(*) See footnote on HLW Technical Waste table. It is possible that the metal component in the waste is underestimated.

Decommissioning Waste (Revised OPERA HLW Technical Waste)

Location	Metal	Metal amount M_j (mol)	Area A_j (m^2)	Notes	Reference
Package Contents (Decommissioning Waste)	Stainless Steel	2.5 kg steel -> 55.911 g/mol -> 4.5E+01 mol stainless steel	3.1E-01	Mass of irradiated metal per ECN container given as 20.9 kg*, assumed to be 50% stainless steel and 50% aluminium by mass. Redistributed inventory across KONRAD** and DDS containers by volume and number of containers (826 KONRAD containers, 4.35 m^3 capacity per container). Surface area estimated assuming 1 mm thick strips, using steel density of 8000 kg/m^3 and aluminium density of 2700 kg/m^3.	Mass of irradiated metal from Section 4.2.2 of Verhoef et al. (2016). Number of KONRAD and DDS containers supplied by email 25/11/22.
	Aluminium (Al)	2.5 kg Al 26.98 g/mol Al -> 9.1E+01 mol Al	9.1E-01		

(*) See footnote on HLW Technical Waste table. It is possible that the metal component in the waste is underestimated.
(**) KONRAD container not included in the analysis

Depleted Uranium

Location	Metal	Metal amount M_j (mol)	Area A_j (m^2)	Notes	Reference
N/A	N/A	N/A	N/A	U is already oxidised, so the only gas-generating process in this case is radiolysis of H_2O. (The KONRAD* container is out of scope.)	

(*) KONRAD container not included in the analysis

Molybdenum Waste

Location	Metal	Metal amount M_j (mol)	Area A_j (m^2)	Notes	Reference
Outer Packaging				None (concrete)	
Package Contents (200L Drum)	Stainless Steel	1.9E+01 kg steel -> 54.911 g/mol -> 3.5E+02 mol galvanised steel	2.4E+00	Outer surface area of 200L drum approximated using simplified cylindrical geometry (diameter 625 mm, height 928 mm). Volume calculated using 1 mm thickness, same as compacted LILW 200L drum. Moles of steel calculated using stainless steel density (8000 kg/m^3). One 200L drum per 1000L container.	Dimensions from Fig 5-4 of Verhoef et al. (2016). Container wall thickness confirmed by email 04/10/22. Galvanised steel density from: https://www.theworldmaterial.com/din-en-10130-dc01-steel-1-0330-material-datasheet/
Package Contents (Reinforcing Steel)	Galvanised Steel	2.0E+02 kg steel -> 55.770 g/mol -> 3.6E+03 mol stainless steel	3.2E+00	Mass derived from maximum steel mass per 1000L (222 kg), total of reinforcing steel + 200L barrel (barrel mass calculated as 19 kg). Estimated total volume from mass and assumed density of 7850 kg/m^3. Estimated surface area from thickness of 8 mm.	Mass from Table 3-4 of Meeussen and Rosca-Bocancea (2014). Steel type given as FeB 500 HKN in Section 5.3.2 of Verhoef et al. (2016) but no information on composition or density found. Steel thickness supplied by email 04/10/22.
Package Contents (Sacrificial Stirrer)	Stainless Steel	6.3E+01 kg steel -> 55.911 g/mol -> 1.1E+03 mol stainless steel	5.2E-01	Total surface area and volume estimated assuming cylindrical geometry with height of 928 mm and radius 30 mm, multiplied by 3 to account for arms. Calculated volume (0.008 m^3) within 0.02 m^3 (200L drum minus 180L waste). Moles of steel calculated assuming density of 8000 kg/m^3.	Dimensions estimated from Fig 5-4 and text in Section 5.3.2 of Verhoef et al. (2016).
Package Contents (Waste – Liquid Molybdenum Waste)	Uranium (U)	N/A	N/A	Radionuclides distributed in a cementitious matrix, so reactive surface area is unclear. Only up to 43 g of U and 6.8 kg of Al, which is small in relation to other metals, so ignored in gas generation calculations. (Contribution to radiolysis is included.)	Mass of uranium and aluminium per waste stream supplied in Table 11 of Filby et al. (2016).
	Aluminium (Al)	N/A	N/A		

Compactible LILW

Location	Metal	Metal amount M_j (mol)	Area A_j (m^2)	Notes	Reference
Outer Packaging (200L Drum)	Galvanised Steel	1.5E+01 kg steel -> 55.770 g/mol -> 2.7E+02 mol galvanised steel	1.9E+00	Outer surface area approximated using simplified cylindrical geometry with no lid (diameter 590 mm, height 880 mm). Volume calculated from 1 mm thickness. Moles of steel calculated from density of 7850 kg/m^3.	Steel type and container thickness from text in Section 5.2.2, dimensions in Fig 5-2 of Verhoef et al. (2016)
Package Contents (Centering Iron)	Stainless Steel	2.7E+00 kg steel -> 55.911 g/mol -> 4.9E+01 mol stainless steel	9.7E-02	Estimated total surface area and volume, assuming cylindrical components. Central rod: radius 10 mm, height 820 mm. Base rods: radius 5 mm, heights 560 mm, 50 mm and 50 mm. Side rods: radius 2 mm, heights 650 mm (x2) and 150 mm (x4). Estimated moles of steel from volume, assuming density 8000 kg/m^3.	Technical drawing of centering iron supplied by email 11/10/22.
Package Contents (5.5x 96 L drum metal)	Galvanised Steel	6.2E-03 m^3 steel (approx. vol of 5.5x 90 L drums of thickness 1 mm) -> 8.7E+02 mol galvanised steel	6.2E+00	No details of 96 L drums indicated in COV023, Fig 5-2 were found. Some details of 90 L drums found in COV023 (e.g. thickness = 1 mm), but no outer dimensions. Same height:diameter ratio as 200 L drum (above) has been assumed to obtain 90 L volume. 5.5 drums per package assumed (average of 4-7 drums shown in COV023, Fig 5-2)	
Package Contents (Waste - Compacted LILW)	Stainless Steel	2.3E+02 kg steel -> 55.911 g/mol -> 4.2E+03 mol stainless steel	2.9E+01	Waste volume calculated from 200L drum inner volume, subtracting 100 mm concrete from top & bottom and 5 mm concrete from sides. Total volume apportioned: metals form 30% of waste matrix, of which 25% aluminium and 75% steel. Moles of steel calculated assuming steel density 8000 kg/m^3. Moles of Al calculated using molar volume 9.99E-6 m^3/mol. Estimated total surface area from calculated volume assuming 1mm thick waste forms (sheets).	Mass derived from Table 5-3 and volume from Fig 5-2 of Verhoef et al. (2016) Molar volume of aluminium from https://periodictable.com/Properties/A/MolarVolume.an.html
	Aluminium (Al)	9.5E+02	9.5E+00		

Non-Compactible LILW

Location	Metal	Metal amount M_j (mol)	Area A_j (m²)	Notes	Reference
Outer Packaging				None (concrete)	
Package Contents (200L Drum)	Stainless Steel	3.5E+02	2.4E+00	As molybdenum	Verhoef et al., 2016; Meeussen and Rosca-Bocancea, 2014
Package Contents (Reinforcing Steel)	Galvanised Steel	3.6E+03	3.2E+00	As molybdenum	Meeussen and Rosca-Bocancea, 2014
Package Contents (Sacrificial Stirrer)	Stainless Steel	1.1E+03	5.2E-01	As molybdenum	Verhoef et al. (2016).

3.2 Organics

Watson (2023) notes that:

- LILW non-compactible waste contains ion exchange resins and other organic materials,
- LILW compactible waste contains plastics and other organic materials, and
- HLW technical waste contains organic materials comprising plastic foils, tissues (paper) and cloths.

Additionally, the revised plans for disposal of HLW Technical waste includes plans for disposal of Legacy Waste in DDS containers, which include a rubber ring. The amount of rubber is small and is ignored in the modelling.

For simplicity, general organic materials in the waste will be treated as cellulose, and so the only organic materials considered in the model are cellulose and ion exchange resins. This is a conservative assumption for plastics, for example, which might only be expected to produce gas via radiolysis and not undergo hydrolysis reactions like cellulose. This is discussed in the following sections.

3.2.1 Cellulose

SMOGG (Swift, 2016) includes a treatment of gas generation from the breakdown of cellulose ($C_6H_{10}O_5$) and isosaccharinic acid (ISA, $C_6H_{12}O_6$). Under neutral conditions, cellulose can undergo microbially-mediated hydrolysis. Under alkaline conditions, cellulose can break down to ISA via the hydrolysis reaction

$$\text{Cellulose} + H_2O \rightarrow \text{ISA}.$$

If the ISA is subsequently transported to neutral regions of the system, it can then undergo degradation, or reduction by nitrate or sulphate to produce CO_2 or CH_4. In the current model, which does not include a detailed spatial discretisation of the near field, it is conservatively assumed that ISA can undergo degradation anywhere in the modelled system.

The SMOGG model (Swift, 2016) includes separate amorphous and crystalline cellulose phases, with distinct ISA breakdown rates for each, and additionally includes 'stopped' amorphous and crystalline phases, which react as follows

$$\text{Stopped amorphous/crystalline cellulose} \leftrightarrow \text{amorphous/crystalline cellulose}.$$

Only the non-stopped cellulose can take part in the hydrolysis reaction.

In the present model, amorphous and crystalline cellulose phases will be represented with stopped phases that cannot undergo hydrolysis. However, for simplicity it will be assumed that the ISA intermediate product of the cellulose degradation reaction

degrades/reduces instantly, so that cellulose breaks down directly to CO_2 and CH_4 by the reactions

$$C_6H_{10}O_{5(am,stop)} \overset{k_{am,d}\ k_{am,s}}{\Longleftrightarrow} C_6H_{10}O_{5(am)}, \quad C_6H_{10}O_{5(am)} + H_2O \xrightarrow{k_{am}} 3CO_2 + 3CH_4$$

$$C_6H_{10}O_{5(cry,stop)} \overset{k_{cry,d}\ k_{cry,s}}{\Longleftrightarrow} C_6H_{10}O_{5(cry)}, \quad C_6H_{10}O_{5(cry)} + H_2O \xrightarrow{k_{cry}} 3CO_2 + 3CH_4$$

Here, $k_{am,s}$ (y^{-1}) are the rate constants for the scission reaction from stopped amorphous cellulose to reactive amorphous cellulose, $k_{am,d}$ (mol kg^{-1} y^{-1}) is the rate constant for the reverse reaction from reactive amorphous cellulose to stopped amorphous cellulose and k_{am} (mol kg^{-1} y^{-1}) is the rate constant for the amorphous cellulose hydrolysis reaction, which is conservatively assumed to apply under alkaline and neutral conditions as described above. The rate constants for crystalline cellulose are named similarly. Values for the rate constants are given in Appendix B.

The simplification of omitting the intermediate ISA product has the advantage of being conservative, in the sense that it provides immediate degradation to gas, so maximises the gas generation rate (provided that the overall cellulose degradation rate is chosen conservatively with respect to each of the 'partial reaction rates'). The amount of gas generated by this mechanism in storage would need to be monitored however, to ensure that a significant amount of gas that might have otherwise been generated under repository conditions is not generated in the operational phase. For added conservatism, from the perspective of post-closure gas generation, it could be assumed that cellulose breakdown can only occur after the waste package is emplaced in the repository, but this is not currently assumed in the model.

The cellulose inventories for the LILW and HLW Technical waste groups are given in Table 3-2. For the compactible LILW, a total mass of cellulose is specified in the OPERA documentation. For the other waste groups, the amount of cellulose has been estimated from the organic content. The notes column in Table 3-2 gives details of how the cellulose inventories per container have been derived for each waste group.

Table 3-2 Amounts of cellulose (moles of $C_6H_{10}O_5$) for each waste group. The initial inventory is assumed to be split evenly between stopped amorphous and crystalline cellulose.

	Total Cellulose per Container (mol)	Notes	References
HLW Technical Waste (OPERA)	4.85E+02	Organic material per waste container 78.6 kg, conservatively assumed to all be cellulose. Molar mass of $C_6H_{10}O_5$ 162 g/mol.	Section 4.2.2 of Verhoef et al. (2016)
Legacy Waste (Revised OPERA HLW Technical Waste)	1.86E+02	Organic inventory of 'HLW Technical Waste' redistributed from 200 ECN containers to 521 DDS drums.	As above
Non-Compactible LILW	0	Organic content is resins rather than cellulose.	
Compactible LILW	6.22E+02	Upper bound of cellulose mass for all LILW in 200L containers given as 1.41E+07 kg. Molar mass of $C_6H_{10}O_5$ 162 g/mol. Divided by number of containers (140,000).	Section 5.13.1.1 of Filby et al. (2016)

3.2.2 Ion Exchange Resins

All nuclear and research reactors in the Netherlands and all facilities for molybdenum production generate waste streams that contain spent ion exchangers. Only the spent ion exchangers from nuclear power plants are conditioned in cement (OPERA-PU-IBR512). These are emplaced in 200 L drum packages.

Spent ion exchange resins are either beads or powder. OPERA-PU-IBR512 quotes research that suggests that it is sensible to assume that the most common type of synthetic ion exchange resin that is used is polystyrene divinylbenzene ($(C_8H_8)_n(C_{10}H_{10})_m$).

Chemical degradation of polymers is initiated by the attack of hydroxyl ions on carbon atoms with a partial positive charge, and so is most significant under alkaline conditions. Carbon atoms with partial positive charge are not usually present in ion exchange resins, which are therefore very resistant to degradation by hydrolysis. Hydrolysis of ion exchange resins is therefore excluded in the model, and so the only impact of ion exchange resins on gas generation is via radiolysis (Section 3.3).

The precise formula unit of polystyrene divinylbenzene is not given in OPERA-PU-IBR512, but given that the overall ratio of C to H in the formula above is 1 to 1, a notional formula unit of $C_{18}H_{18}$ (molar weight = 234.3402 g/mol) can be used to convert between inventory masses and molar amounts for the purposes of determining possible amounts of gas generated from radiolysis (Section 3.3).

Table 3-3 Amounts of ion exchange resin (moles of $C_{18}H_{18}$) for each waste group.

	Total Resin per Container (mol of $C_{18}H_{18}$)	Notes	References
Non-Compactible LILW	8.32E+01	Resin beads (16.8 kg) + powder (2.7 kg) per drum in waste stream II = 19.5 kg/drum. Molar mass of $C_{18}H_{18}$ 234.34 g/mol.	Table 5-9 of Verhoef et al. (2016)

3.3 Radiolysis

Water that is in contact with the waste inside the waste package may be subject to α, β and γ radiolysis and water outside the package may be subject to γ radiolysis, depending on the waste type.

The rate of production of H_2 due to radiolysis of water in location k, $P_{\mathrm{radioH_2O},H_2,k}$ (mol/y) is given by

$$P_{radioH_2O,H_2,k}(t) = \sum_{\nu\in\{\alpha,\beta,\gamma\}} G_{\nu,H_2O,H_2} W^{ADS}_{\nu,H_2O,k}(t)\, \mathcal{T}_{s/y}, \tag{3.15}$$

where G_{ν,H_2O,H_2} (mol/J) is the 'G factor' for water of hydrogen production from radiation of type ν and $W^{ADS}_{\mathrm{v,H_2O,k}}$ (J/s) is the rate of energy absorption by water in location k from radiation of type ν. $\mathcal{T}_{\mathrm{s/y}}$ (s/y) is a second to year scale factor.

The G factors depend on the material subjected to radiolysis. It is assumed that all α and β energy is absorbed within the waste package and a user-specified fraction of the γ energy escapes from the package, so $W^{ADS}_{\alpha,H_2O,out} = W^{ADS}_{\beta,H_2O,out} = 0$.

The energy absorbed by a particular material in the package is calculated as the product of the total decay energy (for α and β radiation) produced in the package and the fraction of the package mass consisting of the material. For γ radiation, a user specified fraction of the decay energy is assumed to escape from the package. For γ radiation absorbed in the package, material mass weighting is again used to determine the energy absorbed by each material. All γ radiation escaping the package is conservatively assumed to be

absorbed by the materials in the region immediately outside the package in which the pore volume V_{out}^{P} (Section 2) is assumed to reside. i.e. no γ radiation is assumed to escape further into the near field. Mass weighting is again used to determine the energy absorbed by each material.

The total mass of solid material inside the package at time t, $M_{waste}(\mathrm{t})$, is

$$M_{waste}(t) = \sum_{j\in\{Metal\,Waste\}} M_j(t) W_{M,j}^{M} + \sum_{l\in\{Organics\}} O_l(t) W_{O,l}^{M} + M_{inert} \tag{3.16}$$

where, $W_{M,j}^{M}$ (kg/mol) is the molar weight of metal j and $W_{O,l}^{M}$ (kg/mol) is the molar weight of organic l and M_{inert} (kg) is the mass of any other material inside the package that is unaccounted for in the metal and organic inventories (e.g. glass and concrete). The total mass in the package is not likely to be greatly affected by corrosion of metals and degradation of organics. Therefore, the total waste mass throughout the simulation is taken to be approximated by the initial waste mass, and so

$$W_{\nu,H_2O,in}^{ADS}(t) = \frac{W_{in}(t) W_{H_2O}^{M}}{M_{waste}(t_s) + W_{in}(t) W_{H_2O}^{M}} f_\nu D_\nu(t) \tag{3.17}$$

where $\mathrm{W}_{\mathrm{H_2O}}^{M}$ (kg/mol) is the molar weight of water and $\mathrm{D}_\nu(t)$ (J/s) is the ν decay power of the waste at time t and f_ν (-) is the fraction of ν decay that remains in the package, with $f_\alpha = f_\beta = 1$ and f_γ being case specific. t_s (y) is the time that the package is placed in storage (Section 2), which represents the start time of the simulation. The rate of energy absorption by water of γ radiation outside the package is

$$W_{\gamma,H_2O,out}^{ADS}(t) = \frac{W_{out}(t) W_{H_2O}^{M}}{M_{surround} + W_{out}(t) W_{H_2O}^{M}} \left(1 - f_\gamma\right) D_\gamma(t), \tag{3.18}$$

where M_{surround} (kg) is the mass of material surrounding the waste package in the model, i.e. in which the pore volume V_{out}^{P} (Section 2) is assumed to reside.

The decay power of the waste at time t for radiation type ν, $D_\nu(t)$ (J/s), in equation (3.17) is given by

$$D_\nu(t) = \sum_{i\in\{rads\}} N_i(t) \lambda_i N_A E_{i,\nu}, \tag{3.19}$$

where the summation is over all radionuclides in the inventory, $N_i(\mathrm{t})$ (mol) is the amount of radionuclide remaining in the inventory at time t, λ_i ($\mathrm{s^{-1}}$) is its decay rate, N_A ($\mathrm{mol^{-1}}$) is Avogadro's constant and $\mathrm{E_{i,\nu}}$ (J/decay) is the energy per decay of type ν for radionuclide i. Average decay energies are given in Appendix C.

The rate of consumption of water in location k due to radiolysis in location k, $Q_{radioH_2O,k}$ (mol/y) is

$$Q_{radioH_2O,k}(t) = \mathcal{S}_{radioH_2O,H_2} P_{radioH_2O,H_2,k}(t), \tag{3.20}$$

where $\mathcal{S}_{radioH_2O,\mathrm{H}_2}$ (-) is the number of moles water consumed in the radiolysis reaction per mole of H_2 that is produced ($\mathcal{S}_{radioH_2O,\mathrm{H}_2} = 1$).

Organic materials may generate H_2, CO_2 and/or CH_4 as a result of radiolysis. Modelling of these process is analogous to the above treatment for radiolysis of water except that generating gas from radiolysis of organics does not impact upon the water inventory, so that there is no contribution to Q_{radioH_2O} from radiolysis of organics.

The rate of production of gas i due to radiolysis of organic phase l, $R_{\mathrm{radio}O_l,H_2}$ (mol/y) is given by

$$P_{radioO_l,i}(t) = \sum_{\nu\in\{\alpha,\beta,\gamma\}} G_{\nu,O_l,i} W^{ADS}_{\nu,O_l}(t)\, \mathcal{S}_y, \tag{3.21}$$

where $G_{\nu,\mathrm{O_l},i}$ (mol/J) is the G factor for organic l of production of gas i from radiation of type ν. $W^{ADS}_{\nu,\mathrm{O_l}}$ (J/s) is the rate of energy absorption by organic l from radiation of type ν, and is given by

$$W^{ADS}_{\nu,O_l}(t) = \frac{O_l(t) W^M_{O_l}}{M_{waste}(t_s) + W_{in}(t) W^M_{H_2O}} f_\nu D_\nu(t). \tag{3.22}$$

Similar to the case for water, if $\mathcal{S}_{radioO_l,i}$ (-) is the number of moles organic l consumed in the radiolysis reaction per mole of gas i that is produced, then the rate at which organic l consumed in the radiolysis reactions, Q_{radioO_l,H_2} (mol/y), is

$$Q_{radioO_l}(t) = \sum_{i\in\{Gases\}} \mathcal{S}_{radioO_l,i} P_{radioO_l,i}(t). \tag{3.23}$$

3.3.1 Radiolysis Factors by Waste Group

f_γ is given for each waste group in Table 3-4. Given a lack of data it is assumed that 99.9% of the gamma energy is contained within the package in all cases. The effect of the assumption can be scoped with a sensitivity analysis, if needed.

G factors for water and organics are waste group independent and are given in Appendix C.

Table 3-4 f_γ factors for each waste group

	f_γ	Notes
Vitrified Waste	0.999	In all cases one thousandth of the gamma energy is assumed to escape the package. This is equivalent to an assumption of a 25mm metallic wall thickness (Watson et al., 2012). Intact and corroded packaging are assumed to perform similarly.
Research Reactor Spent Fuel	0.999	
Uranium Collection Filters	0.999	
Reprocessing Waste	0.999	
HLW Technical Waste (OPERA)	0.999	
Decommissioning Waste (Revised OPERA HLW Technical Waste)	0.999	
Legacy Waste (Revised OPERA HLW Technical Waste)	0.999	
Depleted Uranium	0.999	
Molybdenum Waste	0.999	
Non-Compactible LILW	0.999	
Compactible LILW	0.999	

3.3.2 Radionuclide Inventories

$D_v(t)$ (J/s) in equation (3.19) must be calculated for each waste group by decaying the initial inventory. The initial inventory at the time of disposal (2130) per waste group is provided in Table 3-5. The inventories are calculated from activity data and numbers of packages per waste group listed in Verhoef et al., 2016, 2017.

Table 3-5 Radionuclide inventory (mol) per container at time of disposal (2130) for each waste group. (Blank cells are zero.)

Radionuclide	Vitrified Waste	Research Reactor Spent Fuel	Uranium Collection Filters	Reprocessing Waste	HLW Technical Waste (OPERA)	Decommissioning Waste (Revised HLW Technical Waste)	Legacy Waste (Revised HLW Technical Waste)	Depleted Uranium	Molybdenum Waste	Non-compactible LILW	Compactible LILW
Ac-227	9.99E-13										2.16E-13
Ag-108m				5.15E-11	2.04E-12	4.79E-13	2.26E-14			1.03E-05	4.74E-11
Am-241	3.46E+00	3.67E-01	2.78E-05	1.74E-03	7.97E-05	1.88E-05	8.87E-07		1.01E-08		4.90E-06
Am-242m	1.66E-02			1.66E-06							
Am-243	1.43E+00	1.60E-02	1.21E-03	3.30E-04	3.68E-05	8.66E-06	4.10E-07		4.39E-07		2.03E-10
Be-10										9.13E-06	2.04E-06
Bi-207											8.48E-13
C-14		2.83E-05		5.95E-03	2.34E-04	5.51E-05	2.61E-06			3.06E-03	8.53E-06
Ca-41				2.27E-05	9.02E-07	2.12E-07	1.00E-08			1.54E-05	
Cf-249				8.68E-11							3.50E-12
Cl-36				1.44E-14						9.10E-05	1.03E-06
Cm-243	2.79E-04	2.29E-05	2.79E-06	2.79E-08	8.71E-06	1.99E-06	9.40E-08		1.01E-09		
Cm-244	3.02E-03	2.18E-05	2.65E-06	1.89E-05	8.05E-08	1.89E-08	8.95E-10		9.59E-10		1.93E-11
Cm-245	1.86E-03	7.80E-05	9.51E-06	7.00E-06	2.87E-07	6.76E-08	3.20E-09		3.43E-09		
Cm-246	1.72E-02	5.46E-06	6.66E-07	1.72E-06	2.02E-08	4.75E-09	2.25E-10		2.41E-10		
Cm-247	3.10E-04	2.54E-05	3.10E-06	3.10E-08	9.40E-06	2.21E-06	1.05E-07		1.12E-09		
Cm-248	4.26E-05	3.49E-06	4.26E-07	4.26E-09	1.29E-06	3.04E-07	1.44E-08		1.54E-10		4.81E-11
Co-60										6.02E-12	
Cs-135	5.23E+00	2.97E+00		1.81E-01	7.11E-03	1.67E-03	7.91E-05		1.51E-03	5.22E-04	
Cs-137	7.53E-01	1.39E-01		7.41E-03	1.32E-03	3.11E-04	1.47E-05		6.19E-05	6.84E-05	2.09E-06
Eu-152			8.92E-11	3.96E-09	1.54E-10	3.68E-11	1.74E-12		3.22E-14		2.54E-13
H-3				9.28E-06	4.21E-05	9.90E-06	4.68E-07			1.90E-11	1.01E-08
Ho-166m			3.23E-09								
I-129		3.12E-01	2.45E-09	6.29E-02	7.33E-03	1.73E-03	8.16E-05		1.35E-04	7.12E-04	2.63E-06
K-40											3.99E-03
Kr-81											4.92E-10
Kr-85		4.30E-05			2.94E-06	6.92E-07	3.28E-08				1.11E-11

Mo-93				1.75E-03	6.03E-05	1.62E-05	7.67E-07			1.18E-07	
Nb-93m											1.29E-16
Nb-94		2.06E-06		8.52E-02	3.36E-03	7.91E-04	3.74E-05			7.34E-05	2.35E-09
Ni-59				2.74E+00	8.05E-02	2.55E-02	1.21E-03			3.35E-03	9.01E-08
Ni-63		5.34E-11	7.95E-09	1.33E-01	8.32E-04	1.96E-04	9.26E-06		2.01E-12	1.72E-03	2.80E-06
Np-237	7.78E+00	6.39E-01	2.38E-03	1.26E-03	1.35E-02	3.19E-03	1.51E-04		8.59E-07		4.60E-08
Pa-231		3.49E-06	1.37E-07						4.95E-11		9.83E-10
Pb-210											1.29E-11
Pd-107	3.33E+00	6.37E-02	1.52E-02	3.31E-03	1.55E-03	3.65E-04	1.73E-05		5.51E-06	2.95E-05	
Pm-145			6.14E-14						1.55E-17		
Pu-238	3.17E-03	5.03E-02	1.61E-06	7.96E-03	9.95E-04	2.34E-04	1.11E-05		5.82E-10		4.58E-07
Pu-239	2.62E-01	2.31E+00	3.79E-02	3.90E-01	5.03E-03	1.18E-03	5.60E-05		1.36E-05		2.30E-05
Pu-240	1.15E-01	5.90E-01	5.56E-04	1.83E-01	1.03E-03	2.42E-04	1.14E-05		2.00E-07		4.00E-07
Pu-241	7.97E-05	8.34E-04	5.32E-08	1.53E-04	2.31E-06	5.41E-07	2.56E-08		1.92E-11		3.99E-12
Pu-242	2.86E-02	1.22E-01	2.92E-07	5.93E-02	2.88E-04	6.80E-05	3.22E-06		1.05E-10		5.64E-05
Pu-244	2.97E-03			2.97E-07	9.01E-05	2.12E-05	1.00E-06				
Ra-226	1.25E-11	1.06E-07		1.25E-15	3.22E-09	7.57E-10	3.58E-11				8.09E-07
Re-186m											3.58E-07
Se-79	4.48E-01	3.01E-02	1.04E-03	1.23E-03	4.42E-04	4.72E-04	2.23E-05		8.96E-06	5.35E-05	
Sm-146			8.64E-09								
Sm-147											
Sm-151	3.72E-01	6.02E-02	5.10E-03	3.66E-03	1.37E-04	3.27E-05	1.54E-06		1.84E-06		1.12E-10
Sn-121m										6.57E-09	1.76E-12
Sn-126	6.61E-01	2.65E+00	5.27E-03	1.54E-03	5.89E-04	3.19E-04	1.51E-05		1.50E-05	9.39E-05	
Sr-90	4.46E-01	1.09E-01	9.29E-03	6.01E-03	2.53E-03	5.89E-04	2.78E-05		5.25E-05	1.33E-07	4.22E-08
Tc-99		1.77E+00	2.36E-01	1.46E-01	1.35E+00	3.15E-01	1.49E-02			9.58E-05	1.42E-05
Th-229	6.49E-09	7.27E-09	7.27E-09	6.49E-13	2.20E-10	5.17E-11	2.44E-12				1.25E-10
Th-230	9.57E-07	1.84E-04	1.84E-04	9.57E-11	5.57E-06	1.31E-06	6.19E-08				1.62E-10
U-232	1.54E-05	1.26E-03	1.48E-11	1.54E-09	4.71E-07	1.09E-07	5.18E-09	2.44E-06			8.80E-13
U-233	3.85E-05	2.20E-05	2.25E-07	3.85E-09	6.67E-07	1.57E-07	7.42E-09		8.10E-11		2.46E-08
U-234	8.85E-03	7.41E-01	1.79E-04	5.68E-05	1.58E-02	3.72E-03	1.76E-04	3.21E+00	6.45E-08		9.56E-06
U-235	1.53E-01	2.77E+01	6.76E+01	6.65E-02	7.61E-01	1.79E-01	8.47E-03	1.84E+02	2.44E-02		7.19E-02
U-236	7.45E-02	1.10E+01	8.13E-01	2.14E-02	2.04E-01	4.79E-02	2.27E-03	7.26E+01	2.94E-04		1.51E-07
U-238	1.87E+01	2.54E+02		6.35E+00	1.03E-01	2.43E-02	1.15E-03	5.07E+04	3.23E-03		1.29E+01
Zr-93	1.21E+01	1.93E+00	2.26E-01	1.03E+00	4.07E-02	9.58E-03	4.53E-04		8.15E-05	2.31E-05	

3.4 Water Fluxes

The model tracks the amount of water present inside and outside the package. Water inside can be involved in reactions with the waste and the inner surface of the waste package while water outside can only react with the outer package surface or undergo γ radiolysis. Water inside the waste package can reside in the pore volume and voidage in the waste form. Water outside the package can reside in the pore volume outside the waste package. These are denoted $V_{in}^{P}(t)$ (m^3) and $V_{out}^{P}(t)$ (m^3) respectively. $V_{out}^{P}(t)$ is defined in the scenario model (Section 2).

Water from the geosphere can only enter the two volumes if they are not already fully saturated. The saturations of both locations are denoted $S_{in}(t)$ and $S_{out}(t)$ respectively and are given by

$$S_{in}(t) = \frac{V_{H_2O}^{M} W_{in}(t)}{V_{in}(t)}, \text{ and}$$
$$S_{out}(t) = \frac{V_{H_2O}^{M} W_{out}(t)}{V_{out}(t)}, \tag{3.24}$$

where $V_{H_2O}^{\mathrm{M}}$ (m^3/mol) is the molar volume of water.

The pore volumes are time dependent to allow creep and waste loading and compaction process to be represented if desired. Compressing an already saturated volume would act to expel water from the region. This is ignored in the model for simplicity, but could be added later if it is found to be necessary. Ignoring expulsion of water due to creep is a conservative assumption in the sense that it maximises the potential for reaction of water with the waste. Saturations are therefore capped when evaluating equation (3.24).

The scenario model (Section 2) includes a time $t_{pkg,fail}$ (y) at which the package is assumed to fail mechanically, allowing a larger fraction of the water approaching from the geosphere to directly enter the package.

Total corrosion of the waste package surface is monitored in the corrosion model (Section 3.1). After the outer surface is completely corroded the water flux approaching the exterior of the package can directly approach the interior (this conservatively assumes the exterior is already saturated), which will increase the potential for waste-water reactions, unless the waste is already saturated. If the waste is already saturated the incoming water is redirected outside of the package. If the outside of the package is already saturated then any additional incoming water is ignored. Corrosion is monitored via the $f_{\mathrm{pkg,corrode}}$ (-) quantity, which represents the fraction of the thickness of the outer packaging that is corroded. $f_{\mathrm{pkg,corrode}}$ is initially zero, and when $f_{\mathrm{pkg,corrode}} = 1$ the outer packaging is assumed to be fully corroded, so that all water approaching from the geosphere is assumed to directly enter the package (the pore volume outside the package being conservatively assumed to be fully saturated).

The flux of water directly entering the package from the geosphere, $Q_{pkg,geo}$ (mol/y) is therefore given by

$$Q_{pkg,geo} = \begin{cases} \begin{cases} f_{pkg,init} Q_{geo} H(1 - S_{in}) & t < t_{pkg,fail} \\ f_{pkg,fail} Q_{geo} H(1 - S_{in}) & t \geq t_{pkg,fail} \end{cases} & f_{pkg,corrode} < 1 \\ Q_{geo} H(1 - S_{in}) & f_{pkg,corrode} = 1 \end{cases}, \quad (3.25)$$

and the flux of water approaching the exterior of the package, which can react with the package surface, $Q_{surf,geo}$ (mol/y) is given by

$$Q_{surf,geo} = \begin{cases} \begin{cases} (1 - f_{pkg,init}) Q_{geo} H(1 - S_{out}) & t < t_{pkg,fail} \\ (1 - f_{pkg,fail}) Q_{geo} H(1 - S_{out}) & t \geq t_{pkg,fail} \end{cases} & f_{pkg,corrode} < 1 \\ Q_{geo}\big(1 - H(1 - S_{in})\big) H(1 - S_{out}) & f_{pkg,corrode} = 1 \end{cases}. \quad (3.26)$$

The Heaviside functions are smoothed in the implementation. For numerical stability, the switch when $f_{pkg,corrode} = 1$ in equations (3.25) and (3.26) is replaced by a gradual ramping of the flux between $f_{pkg,corrode} = 0.99$ and $f_{pkg,corrode} = 1$, as described in Section 3.1 when $f_{pkg,corrode}$ is introduced (equation (3.9)).

As noted in Section 2, the gradual shutting down of inflows due to pressurisation of the excavation is conservatively ignored in the central analysis case, but can be imposed on the model by setting Q_{geo} to be a function of time.

In addition to the geosphere fluxes, after complete corrosion of the waste package if there is water present outside of the waste package and if the inside of the waste package is not fully saturated, then a kinetic rate Q_{out_in} (mol/y) is applied to transfer any water from the outside to the interior of the package to promote reactions with the waste. Q_{out_in} is given by

$$Q_{out\_in} = \begin{cases} k_{out\_in} W_{out} & \text{when } S_{in} < 1 \text{ and } S_{out} > 0, \\ 0 & \text{otherwise,} \end{cases} \quad (3.27)$$

where k_{out_in} (y^{-1}) is a rate constant that controls the transfer of the water from the outside of the package to the inside. By default, this is set conservatively to 10^2 (y^{-1}) to approximate an instantaneous[2] transfer of water from outside of the package to the inside whenever water is available outside and when there is unsaturated pore/void space available inside the package. A smaller value could be used to approximate a permeability-controlled water availability.

[2] It may be necessary to choose a smaller value if numerical convergence problems are encountered.

3.5 Governing Equations

The model solves for the following quantities:

- The remaining amount of metal j at time t, $M_j(t)$ (mol),
- The amount of water in location k at time t, $W_k(t)$ (mol),
- The amount of organics of type l at time t, $O_l(t)$, and
- The cumulative amount of gas of type i produced at time t, $G_i(t)$ (mol),

where, as noted earlier, the index j on metals denotes (metal, usage, geometry) combinations, the index k on water denotes the location, being either inside or outside the package, and the indices l and i are over organic and gas species respectively.

Source and sink terms for each of the modelled quantities are described in the preceding Sections 3.1- 3.3 and water fluxes into the modelled system were described in Section 3.4. These combine to form the following governing equations for the modelled quantities:

$$\frac{dM_j}{dt} = -R_{corr,j} \quad \forall\, j \in \{\text{Metal types, usages and geometries}\}, \tag{3.28}$$

$$\begin{aligned} \frac{dW_{in}}{dt} &= Q_{pkg,geo} - Q_{corr,in} - Q_{radioH_2O,in} + Q_{out\_in} \\ \frac{dW_{out}}{dt} &= Q_{surf,geo} - Q_{corr,out} - Q_{radioH_2O,out} - Q_{out\_in} \end{aligned} \tag{3.29}$$

$$\frac{dO_l}{dt} = -Q_{radioO_l} - R_{org,l} \quad \forall\, l \in \{\text{Organics}\}, \tag{3.30}$$

$$\begin{aligned} \frac{dG_i}{dt} = P_{corr,i} + P_{org,i} + \sum_{k\in\{in,out\}} P_{radioH_2O,i,k} \\ + \sum_{l\in\{Organics\}} P_{radioO_l,i} \quad \forall\, i \in \{\text{Gases}\}, \end{aligned} \tag{3.31}$$

(N.B. $P_{radioH_2O,i,k} = 0$ for $i \neq H_2$.)

In (3.30) and (3.31), $R_{org,l}$ and $P_{org,i}$ (mol/y) are the rate of degradation of organic material l and the rate of production of gas i due to degradation of organics respectively. In the current model these are only composed of contributions from the degradation of cellulose (Section 3.2.1) since in the current model it is assumed that degradation of ion exchange resins does not result in the generation of gas (Section 3.2.2). The total gas amount G_i in (3.31) is accumulated as separate components $G_{i,in}$ and $G_{i,out}$.

3.6 Package Physical Properties

Parameters representing other quantities that are required to define the waste packages for each waste group are listed in Table 3-6.

The 'References & Notes' column gives details about how these quantities were derived for each waste group. In general, the pore volume and voidage have been estimated from the dimensions of the containers and contents, and assuming any concrete or grout has a porosity of 20% (where not otherwise specified in the OPERA documentation). The initial water content is assumed to be 0 for all closed packages, unless there is concrete present in the inventory (in which case the pore space is assumed to be 80% saturated unless otherwise specified in the OPERA documentation).

Table 3-6 Summary of package-specific quantities in the package-scale gas generation model

	Water Quantities					Package Ventilation	Packaging Material	References & Notes
	$V_{in}^{P}(t)$	$W_{in}(0)$	M_{inert}	CementMtx		Vented	j^{*}	
				In Package	Outside Package			
Units	m^3	mol	kg	-	-	-	- (name)	
Description	Pore volume and voidage in the waste form. Time dependent to allow package loading/compaction processes to be represented, if required.	Initial water inventory in the package	Total mass of inert materials in the package, e.g. glass, concrete, …	Flag indicating presence of a cement matrix in the waste form or outside the waste form.		Flag indicating whether packages are open/vented (1) or closed (0).	Metal from which the outer packaging is constructed.	
Vitrified Waste	7.5E-02	0.0E+00	3.8E+02	0	0	0	Stainless Steel	Inert material is 380 kg glass (Table 3-8 Meeussen and Rosca-Bocancea, 2014). Void space estimated from voidage between glass and container.
Research Reactor Spent Fuel	4.7E-03	0.0E+00	0.0E+00	0	0	0	Stainless Steel	Estimated voidage between metal components (average of LEU and HEU).
Uranium Collection Filters	7.9E-02	0.0E+00	0.0E+00 (No data for mass of filters)	0	0	0	Stainless Steel	Estimated voidage in aluminium drums between filter houses

Reprocessing Waste	3.9E-02	0.0E+00	0.0E+00	0	0	0	Stainless Steel	Section 4.1.1 of Verhoef et al. (2016), void space around 20% of apparent waste volume.
HLW Technical Waste (OPERA)	3.7E-02	1.7E+03	4.3E+02	1	0	0	Stainless Steel	Assume concrete porosity 20%, 50 mm of concrete surrounding waste (Fig 4-3 of Verhoef et al., 2016). Assume saturation 80%. Assume concrete density 2300 kg/m^3.
Decommissioning Waste (Revised OPERA HLW Technical Waste)	3.5E+00*	8.4E-03	2.2E+00	0	N/A (0)	N/A (0)	N/A (KONRAD excluded from analysis)	Voidage estimated from volume of ECN compacted pucks and capacity of KONRAD/DDS container. Concrete content from Table 3-11 of Meeussen and Rosca-Bocancea, 2014 (waste matrix only). KONRAD package for the decommissioning waste not included in analysis.
Legacy Waste (Revised OPERA HLW Technical Waste)	1.7E-01	4.0E-04	1.0E-01	0	1	1	Stainless Steel	
Depleted Uranium	2.16E-01 (No data, so assume initial water fills void volume)	1.2E+04	1.5E+03	1	N/A (0)	N/A (0)	N/A (KONRAD excluded from analysis)	Water content and inert mass from Table 5-1 of Verhoef et al. (2016). Konrad package not included in analysis.

Molybdenum Waste	1.7E-01	9.6E+03	2.1E+03	1	0	1	Stainless Steel	Assuming 20% voidage of 200L drum (180L waste in 200L drum) minus volume of stirrer, plus concrete porosity (1000L drum minus 200L drum minus reinforcing steel). Water content of waste from Table 5-5 and concrete from Table 5-4 of Verhoef et al. (2016).
Non-Compactible LILW	1.7E-01	9.4E+03	2.1E+03	1	0	1	Stainless Steel	Similar to molybdenum wastes. Water is assumed to fill voidage.
Compactible LILW	1.7E-02	8.7E+02	2.0E+02	1	0	1	Galvanised Steel	Water content from Table 5-4 of Verhoef et al. (2016), concrete volume from Fig 5-2.

(*) The resulting waste porosity is ~80%. As noted in the corresponding table in Section 3.1.1 it is suspected that the metal inventory is underestimated for this waste group. Additionally, it is suspected that other decommissioning materials (e.g. concrete) may be present in the packages. More information is needed on the revised waste groups in order to improve the estimates.

(Input quantities that can be time dependent are denoted as functions of time.)

4 Summary

Sections 2 and 3 present a specification for a package-scale gas generation model. The model is intentionally simplistic and is designed to allow scoping calculations to be performed to provide plausible gas generation rates and amounts from the various waste groups that will be disposed in COVRA's repository. The waste overpacks are being considered by COVRA in a separate modelling study and are not included in the model, but their effect should be considered when specifying input parameters, e.g. to the rate of inflow of water from the geosphere (Q_{geo}), which should account for consumption of water in reactions with the overpack before it reaches the package.

The model includes a number of simplifications, which can be made more realistic in future iterations of the model if it is found necessary in order to more closely bound the likely gas generation rates in the repository. The simplifications in the model, several of which could be easily updated include:

- No coupling of groundwater inflow rates to pressurisation of the repository (pressurisation would be expected to reduce the rate of inflow - this can be accounted for via a time-dependent specification of Q_{geo} in the current formulation of the model, but could be more tightly coupled in a future update),
- Requirement for complete corrosion of the outer packaging before it is considered to be breached for flow (the effect can be approximated by imposing mechanical failure on the model with $t_{pkg,fail}$ and $f_{pkg,fail}$),
- The transition between neutral-alkaline, low-chloride-high-chloride and oxic-anoxic conditions in the pore water is assumed to be instant rather than being represented with a transient,
- Metal corrosion is modelled using a single rate, rather than periods of acute and chronic corrosion,
- Treatment of all metal components with a plate geometry,
- Simplification of the cellulose degradation under alkaline conditions to ignore intermediate degradation to ISA.

A central analysis case parameterisation of the model for COVRA's eleven waste groups is provided. The central analysis case is intended to be generally conservative and includes the following assumptions:

- Geosphere inflow rates are constant at 1 g/m/day (based on modelled inflows a WIPP from the DECOVALEX 2023 project),
- Different metal waste features composed of the same metals are treated as a single bulk metal,
- All general organic waste material is treated as cellulose, and

- No radiolysis is assumed during the storage period (this is a non-conservative assumption, which is made due to a lack of data – radionuclide inventories for the different waste groups are only available from 2130).

High-level results from an early version of the central analysis case are shown in the verification calculations in Appendix D. The results are explored in more detail in Benbow et al. (2023).

References

References cited in the main text and in Appendices A-D are listed below.

Benbow S, Watson S, Newson R, Bruffel L and Bond A (2023), *Potential Gas Generation in a Salt Repository: Gas Generation Model – Results*. Quintessa report to COVRA QDS-10075A-T3-RESULTS v1.0.

Filby A, Deissmann G, Wiegers R (2016), *LILW degradation processes and products.* OPERA-PU-IBR512.

GTG. (2017), *GoldSim® User's Guide Version 12.0*. GoldSim® Technology Group. Issaquah, WA. February 2017.

Guiltinan E, Bartol J, Benbow S, Bourret M, Czaikowski O, Jantschik K, Jayne R, Kuhlman K, Norris S, Rutqvist J, Shao H, Tounsi H, Watson C and Stauffer P (2022), *Brine Availability Test in Salt: Collaborative Modeling Within DECOVALEX*. International High-Level Radioactive Waste Management 2022, Phoenix, USA.

Hoch A, Smart N, Wilson J and Reddy B (2010), *A Survey of Reactive Metal Corrosion Data for Use in the SMOGG Gas Generation Model*. Serco report to RWM, SA/ENV-0895, Issue 2.

ICRP (2008), *Nuclear Decay Data for Dosimetric Calculations.* ICRP Publication 107. Ann. ICRP 38 (3).

Meeussen J C L, Rosca-Bocancea E (2014), *Determination of the inventory: part B matrix composition.* OPERA-PU-NRG1112B.

Quintessa (2013). *QPAC: Quintessa's General-Purpose Modelling Software.* QRS-QPAC-11, http://www.quintessa.org/qpac-overview-report.pdf

Smart N and Hoch A (2010), *A Survey of Steel and Zircaloy Corrosion Data for Use in the SMOGG Gas Generation Model*, Serco report to RWM, SA/ENV-0841 Issue 3.

Smit, H., 2022. *Long term disposal of nuclear waste in the Netherlands: possibilities and questions to be asked*. (COVRA)

Swift B T (2016), *Specification for SMOGG Version 7.0: A Simplified Model of Gas Generation from Radioactive Waste*. AMEC report to RWM AMEC/204651/001 Issue 2.

Swift B T and Rodwell W R (2006), Specification for SMOGG Version 5.0: a Simplified Model of Gas Generation from Radioactive Wastes. Serco report to RWM SERCO/ERRA-0452 Version 6.

Verhoef E V, Neeft E A C, Deissmann G, Filby A, Wiegers R B, Kers D A (2016), *Waste families in OPERA*. OPERA-PG-COV023.

Verhoef E, Neeft E, Chapman N and McCombie C (2017), *OPERA Safety Case*.

Watson S (2023), *Potential Gas Generation in a Salt Repository: Waste Groups and High-Level Conceptualisation*. Quintessa report to COVRA QDS-10075A-T1-WASTES v1.0.

Watson S, Benbow S, Suckling P, Towler G, Metcalfe R, Penfold J, Hicks T, Pekala M (2012), *Assessment of Issues Relating to Pre-Closure to Post-closure Gas Generation in a GDF*. Quintessa report to RWM QRS-1378ZP-R1, Issue 3.

Appendix A Metal Corrosion Rate Parameters

Parameter values to be used in the modelling of corrosion using the approach described in Section 3.1 are given in Table A-1. All possible combinations of porewater conditions are shown in the table, but combinations that are not relevant to the simplified model presented in Section 3.1 are greyed-out, and data are not given.

Table A-1 Metal corrosion rate data for the different porewater conditions (oxic/anoxic, high chloride / low chloride, alkaline/neutral). Porewater condition combinations and parameters that are greyed out are not relevant to the current modelling.

Metal	Condition	Reaction	k_e (mol/m²/y)	Temperature Scaling Factor	Reference
Stainless Steel	Anox,HighCl,Alk	3 Fe + 4 H_2O -> Fe_3O_4 + 4 H_2	1.46E-03 (1.00E-08 m/y)	(None)	Watson et al. (2012)
	Anox,HighCl,Neut		1.46E-02 (1.00E-07 m/y)	(None)	Watson et al. (2012)
	Anox,LowCl,Alk		1.46E-03 (1.00E-08 m/y)	(None)	Smart and Hoch (2010)
	Anox,LowCl,Neut		1.46E-02 (1.00E-07 m/y)	(None)	Smart and Hoch (2010) and by analogy with Watson et al. (2012)
	Oxic,HighCl,Alk				
	Oxic,HighCl,Neut				
	Oxic,LowCl,Alk	3 Fe + 2 O_2 -> Fe_3O_4	2.91E-03 (2.00E-08 m/y)	1 (20C), 2.714 (35C), 6.716 (50C), 32.632 (80C)	Watson et al. (2012)
	Oxic,LowCl,Neut		2.91E-03 (2.00E-08 m/y)	1 (20C), 2.714 (35CC), 6.716 (50C), 32.632 (80C)	Watson et al. (2012)
Carbon/mild steel (and galvanised steel – protective plating is conservatively ignored)	Anox,HighCl,Alk	3 Fe + 4 H_2O -> Fe_3O_4 + 4 H_2	1.41E-02 (1.00E-07 m/y)	(None)	Watson et al. (2012)
	Anox,HighCl,Neut		4.22E+00 (3.00E-05 m/y)	(None)	Watson et al. (2012)
	Anox,LowCl,Alk		1.41E-02 (1.00E-07 m/y)	(None)	Watson et al. (2012)
	Anox,LowCl,Neut		4.22E+00 (3.00E-05 m/y)	(None)	Watson et al. (2012)
	Oxic,HighCl,Alk				
	Oxic,HighCl,Neut				
	Oxic,LowCl,Alk	3 Fe + 2 O_2 -> Fe_3O_4	1.41E-02 (1.00E-07 m/y)	1 (20C), 1.461 (35C), 2.062 (50C), 3.76 (80C)	Watson et al. (2012)

	Oxic,LowCl,Neut		4.22E+00 (3.00E-05 m/y)	1 (20C), 1.461 (35C), 2.062 (50C), 3.76 (80C)	Watson et al. (2012)
Zircaloy	Anox,HighCl,Alk	Zircaloy + 2 H_2O -> ZrO_2 + 2 H_2	7.25E-05 (1.00E-09 m/y)	1 (30C), 1.459 (35C), 3 (45C), 4.23 (50C), 27.088 (50C)	Watson et al. (2012)
	Anox,HighCl,Neut		7.25E-05 (1.00E-09 m/y)	1 (30C), 1.459 (35C), 3 (45C), 4.23 (50C), 27.088 (50C)	Watson et al. (2012)
	Anox,LowCl,Alk		7.25E-05 (1.00E-09 m/y)	1 (30C), 1.459 (35C), 3 (45C), 4.23 (50C), 27.088 (50C)	Watson et al. (2012)
	Anox,LowCl,Neut		7.25E-05 (1.00E-09 m/y)	1 (30C), 1.459 (35C), 3 (45C), 4.23 (50C), 27.088 (50C)	Watson et al. (2012)
	Oxic,HighCl,Alk				
	Oxic,HighCl,Neut				
	Oxic,LowCl,Alk	Zircaloy + 2 H_2O -> ZrO_2 + 2 H_2	7.25E-03 (1.00E-07 m/y)	1 (20C), 2.282 (35C), 5.207 (50C), 27.113 (80C)	Smart and Hoch (2010) (Nirex 97 value)
	Oxic,LowCl,Neut		7.25E-03 (1.00E-07 m/y)	1 (20C), 2.282 (35C), 5.207 (50C), 27.113 (80C)	Smart and Hoch (2010) (Nirex 97 value)
Aluminium	Anox,HighCl,Alk	2 Al + 6 H_2O -> 2 $Al(OH)_3$ + 3 H_2	2.45E+00 (2.45E-05 m/y)	(None)	Watson et al. (2012)
	Anox,HighCl,Neut		1.00E-02 (1.00E-07 m/y)	(None)	Hoch et al. (2010)
	Anox,LowCl,Alk		2.45E+00 (2.45E-05 m/y)	(None)	Watson et al. (2012)
	Anox,LowCl,Neut		1.00E-02 (1.00E-07 m/y)	(None)	Hoch et al. (2010)
	Oxic,HighCl,Alk				
	Oxic,HighCl,Neut				
	Oxic,LowCl,Alk	2 Al + 6 H_2O -> 2 $Al(OH)_3$ + 3 H_2	2.45E+00 (2.45E-05 m/y)	(None)	Watson et al. (2012)
	Oxic,LowCl,Neut		1.00E-02 (1.00E-07 m/y)	(None)	Hoch et al. (2010)

Appendix B Organic Degradation Reaction Parameters

Reaction rates in the cellulose degradation reaction are listed in Table B-1.

Table B-1 Rate constants for cellulose degradation reactions, from Watson et al. (2012).

Rate Parameter	Rate (y^{-1})
$k_{am,s}$	1.7E-04
$k_{am,d}$	8.8E-03
k_{am}	8.8E-01
$k_{cry,s}$	1.7E-05
$k_{cry,d}$	4.4E-05
k_{cry}	4.4E-03

Appendix C Radiolysis Reaction Parameters

G factors for radiolysis of water for hydrogen production are given in Table C-1.

G factors for radiolysis of organics for H_2, CO_2 and CH_4 production are given in Table C-2.

Average decay energies per radionuclide are given in Table C-3.

Table C-1 G factors for radiolysis of water (Watson et al., 2012)

ν	G_{ν,H_2O,H_2} (mol/J)
α	1.7E-07
β	5.2E-08
γ	5.2E-08

Table C-2 G factors for radiolysis of organics (Watson et al., 2012). G factors for ISA are used for cellulose → CO_2 and CH_4; G factors for polymers are used for resins → H_2 and G factors for ISA are used for resins → CH_4.

ν	G factors for cellulose (mol/J)			G factors for resins (mol/J)		
	$G_{\nu,\text{cellulose},H_2}$	$G_{\nu,cellulose,CO_2}$	$G_{\nu,cellulose,CH_4}$	$G_{\nu,\text{resins},H_2}$	$G_{\nu,resins,CO_2}$	$G_{\nu,resins,CH_4}$
α	1.5E-07	4.1E-07	1.5E-07	2.8E-07	-	1.5E-07
β	6.2E-07	5.6E-07	4.0E-07	6.2E-07	-	4.0E-07
γ	3.3E-07	5.7E-07	4.0E-07	6.2E-07	-	4.0E-07

Table C-3 Radionuclide average decay energies. (Blank cells are zero.)

Radionuclide	Average Decay Energy (J/decay)			Reference
	α	β	γ	
Ac-225	4.48E-12	1.11E-13	3.56E-14	Swift, 2016
Ac-227	1.11E-14	3.21E-15	2.20E-16	Swift, 2016
Ag-108m		1.10E-14	2.61E-13	Swift, 2016
Am-241	8.92E-13	6.28E-15	4.51E-15	Swift, 2016
Am-242m	3.80E-15	3.57E-14	4.02E-15	Swift, 2016
Am-243	8.57E-13	4.59E-14	3.83E-14	Swift, 2016
Be-10		4.04E-14		Swift, 2016
Bi-207	1.91E-14	2.46E-13	2.65E-13	ICRP 107
C-14		7.92E-15		Swift, 2016
Ca-41		4.55E-16	6.99E-17	Swift, 2016
Cf-249	9.49E-13	4.78E-15	5.27E-14	Swift, 2016
Cl-36		3.94E-14	4.35E-18	Swift, 2016
Cm-242	9.92E-13	1.63E-15	2.20E-16	Swift, 2016
Cm-243	9.50E-13	2.23E-14	2.13E-14	Swift, 2016

Cm-244	9.43E-13	1.38E-15	2.08E-16	Swift, 2016
Cm-245	8.72E-13	1.30E-14	1.50E-14	Swift, 2016
Cm-246	8.82E-13	1.31E-15	4.80E-16	Swift, 2016
Cm-247	8.05E-13	3.14E-14	5.25E-14	Swift, 2016
Cm-248	3.17E-12	1.01E-15	9.27E-14	Swift, 2016
Co-60		1.55E-14	4.01E-13	Swift, 2016
Cs-135		1.07E-14		Swift, 2016
Cs-137		3.94E-14	9.06E-14	Swift, 2016
Eu-152	2.72E-13	2.07E-14	1.86E-13	Swift, 2016
H-3		9.13E-16		Swift, 2016
Ho-166m		1.64E-14	2.77E-13	Swift, 2016
I-129		8.82E-15	3.69E-15	Swift, 2016
K-40		8.35E-14	2.52E-14	Swift, 2016
Kr-81		8.62E-16	1.18E-15	Swift, 2016
Kr-85		4.01E-14	3.57E-16	Swift, 2016
Mo-93		9.04E-16	1.75E-15	Swift, 2016
Nb-93m		4.63E-15	3.13E-16	Swift, 2016
Nb-94		2.69E-14	2.52E-13	Swift, 2016
Ni-59		2.74E-15		Swift, 2016
Ni-63		2.74E-15		Swift, 2016
Np-237	7.78E-13	1.12E-14	5.36E-15	Swift, 2016
Pa-231	8.10E-13	8.37E-15	6.20E-15	Swift, 2016
Pa-233		3.14E-14	3.45E-14	Swift, 2016
Pb-210	1.00E-18	6.84E-14	9.15E-16	Swift, 2016
Pd-107		1.51E-15		Swift, 2016
Pm-145	1.04E-21	1.95E-15	5.05E-15	Swift, 2016
Po-210	8.65E-13	1.34E-20	1.42E-18	Swift, 2016 / Swift and Rodwell, 2006*
Pu-238	8.93E-13	1.79E-15	2.48E-16	Swift, 2016
Pu-239	8.38E-13	1.19E-15	1.13E-16	Swift, 2016
Pu-240	8.39E-13	1.78E-15	2.18E-16	Swift, 2016
Pu-241	1.92E-17	8.39E-16	8.27E-19	Swift, 2016
Pu-242	7.96E-13	1.50E-15	2.07E-16	Swift, 2016
Pu-244	7.80E-13	9.91E-14	2.02E-13	Swift, 2016
Ra-223	4.30E-12	1.65E-13	4.95E-14	Swift, 2016
Ra-225		1.73E-14	2.21E-15	Swift, 2016
Ra-226	3.90E-12	1.49E-13	2.87E-13	Swift, 2016
Re-186m	2.03E-14	3.32E-15	2.36E-14	ICRP 107
Sb-126		5.32E-14	4.41E-13	Swift, 2016
Se-79		8.41E-15		Swift, 2016
Sm-146	4.05E-13			ICRP 107
Sm-147	3.70E-13			Swift, 2016
Sm-151		3.18E-15	2.29E-18	Swift, 2016
Sn-121m		2.00E-14	8.15E-16	Swift, 2016
Sn-126		1.20E-13	2.61E-13	Swift, 2016
Sr-90		1.80E-13	4.92E-16	Swift, 2016
Tc-99		1.62E-14	1.12E-19	Swift, 2016
Th-227	9.63E-13	7.89E-15	1.76E-14	Swift, 2016

Th-228	5.21E-12	1.46E-13	2.37E-13	Swift, 2016
Th-229	7.92E-13	1.85E-14	1.45E-14	Swift, 2016
Th-230	7.60E-13	1.98E-15	2.04E-16	Swift, 2016
Th-234		1.40E-13	4.91E-15	Swift, 2016
U-232	8.64E-13	2.69E-15	2.70E-16	Swift, 2016
U-233	7.85E-13	1.22E-15	1.96E-16	Swift, 2016
U-234	7.75E-13	2.26E-15	2.32E-16	Swift, 2016
U-235	7.14E-13	3.40E-14	3.10E-14	Swift, 2016
U-236	7.30E-13	1.62E-15	1.90E-16	Swift, 2016
U-238	6.82E-13	1.69E-15	2.01E-16	Swift, 2016
Zr-93		3.06E-15		Swift, 2016

(*) β decay energy of Po-210 in Swift (2016) is stated to be 1.34E-02, which appears to be a typographical error. Value of 1.34E-20 used here is taken from Swift and Rodwell (2006).

Appendix D Verification

A gas generation model based on the specification in Sections 2 and 3 has been implemented using Quintessa's QPAC software (Quintessa, 2013). A separate implementation by an independent team has been developed using the GoldSim ® software (GTG, 2017). The results of a preliminary version of the results of the model applied to the central analysis case have been compared for each of the waste groups considered in order to verify the implementations of the model. The preliminary version of the central analysis case differs only from the finalised version in that it mis-classifies stainless steel and galvanised components of the molybdenum and non-compactible LILW waste groups, it incorrectly assumes a steel outer package on the 1000 L concrete drum and omits the steel filters in the uranium collection filters case. The differences do not significantly affect the phenomenology of the results. Since this appendix focusses only on the verification of the implementation of the models and not the parameterisation it is a suitable verification problem. A discussion of the details of the results of the (finalised) central analysis case, and a range of sensitivity cases, with implications for disposal are given in Benbow et al. (2023). That modelling uses the QPAC implementation of the model.

Figure D-1 to Figure D-10 show the calculated evolutions from both the QPAC and GoldSim ® models of the inventories of metals (top-left), organics (top-right), water inside and outside the package (bottom-left) and amount of gas produced inside and outside the package (bottom-right) for the ten waste groups that are considered. The pink shaded region indicates the storage period, and the grey shaded region indicates the period after disposal. An overall period of 10^6 y is simulated, with the storage period assumed to last for the first 100 y. The QPAC model is configured to simulate each waste group separately, with each calculation typically taking 1-2 seconds on a modern PC. The GoldSim ® model is configured to simulate all waste groups in the same repository level simultaneously (i.e. 5 or 6 cases simultaneously). It takes approximately 20-30 minutes to run. When running cases for single waste groups it has been found that care has to be taken with the GoldSim ® solver to ensure that all features of the evolution are captured. The plots are generated using post-processing scripts coded in Python.

Good agreement is seen between the QPAC and GoldSim ® implementations for all the calculated quantities for each case. Not every case includes all possible processes (e.g. only three cases include cellulose in the waste form) but collectively they span the set of processes that are implemented.

Some differences in water amounts are seen between the models when saturations approach zero due to the different approaches to handling the rate limiting of water-consuming processes when saturations are small (see, for example, the results for the compactible LILW case shown in Figure D-10). However, the impact of these differences is negligible in terms of the rates at which metals and organics are consumed and

therefore the rate at which gases are produced, as seen in the associated metal, organics and gas inventories.

The similarity between the results lends confidence that the models are implemented consistent with the specification in Sections 2 and 3.

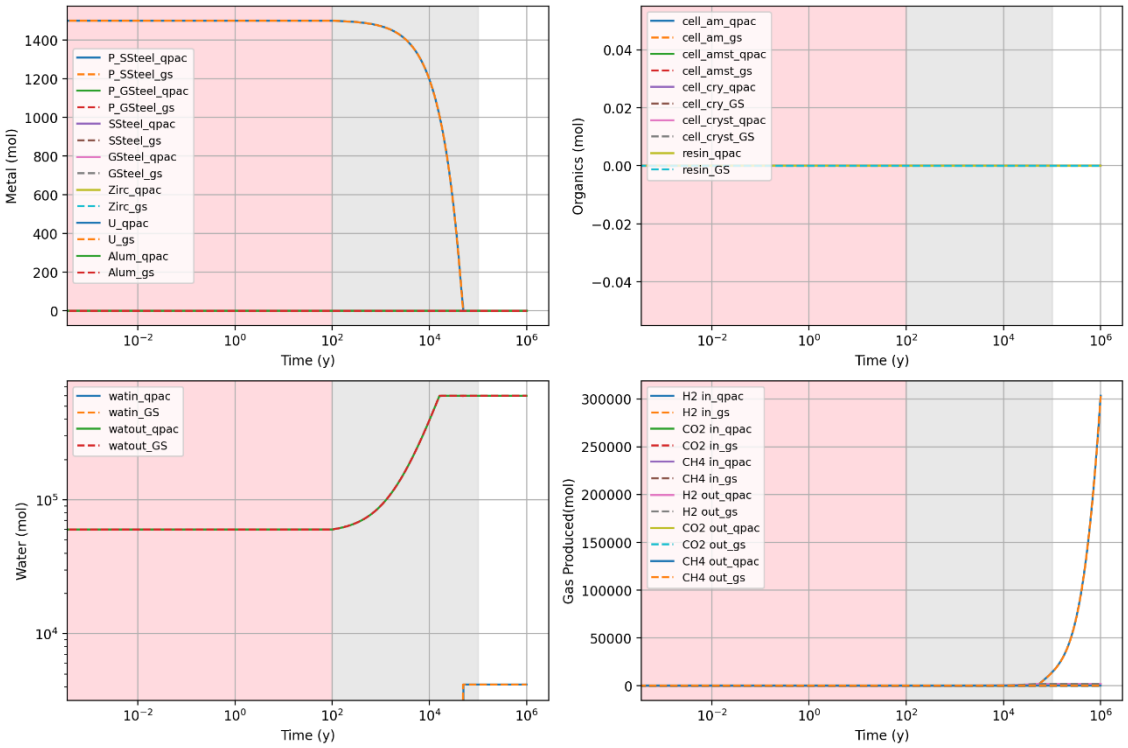

Figure D-1 Vitrified waste: metals inventory (top-left); organics inventory (top-right); water inventory (bottom-left); and amounts of gas produced (bottom-right).

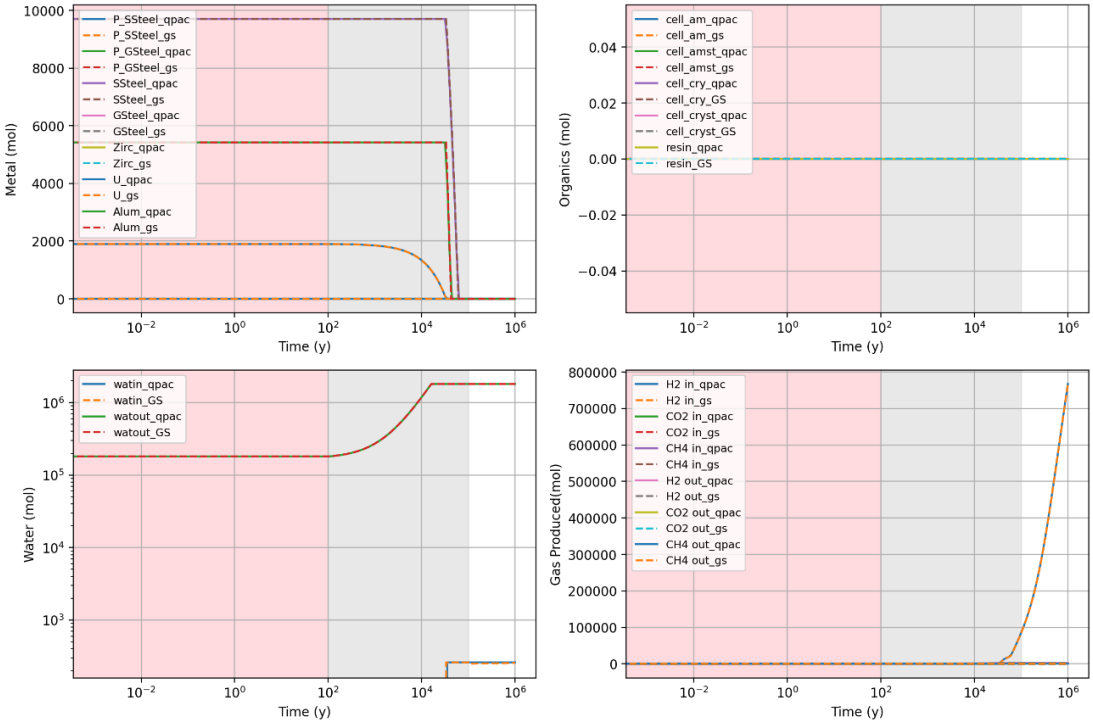

Figure D-2 Research Reactor Spent Fuel: metals inventory (top-left); organics inventory (top-right); water inventory (bottom-left); and amounts of gas produced (bottom-right).

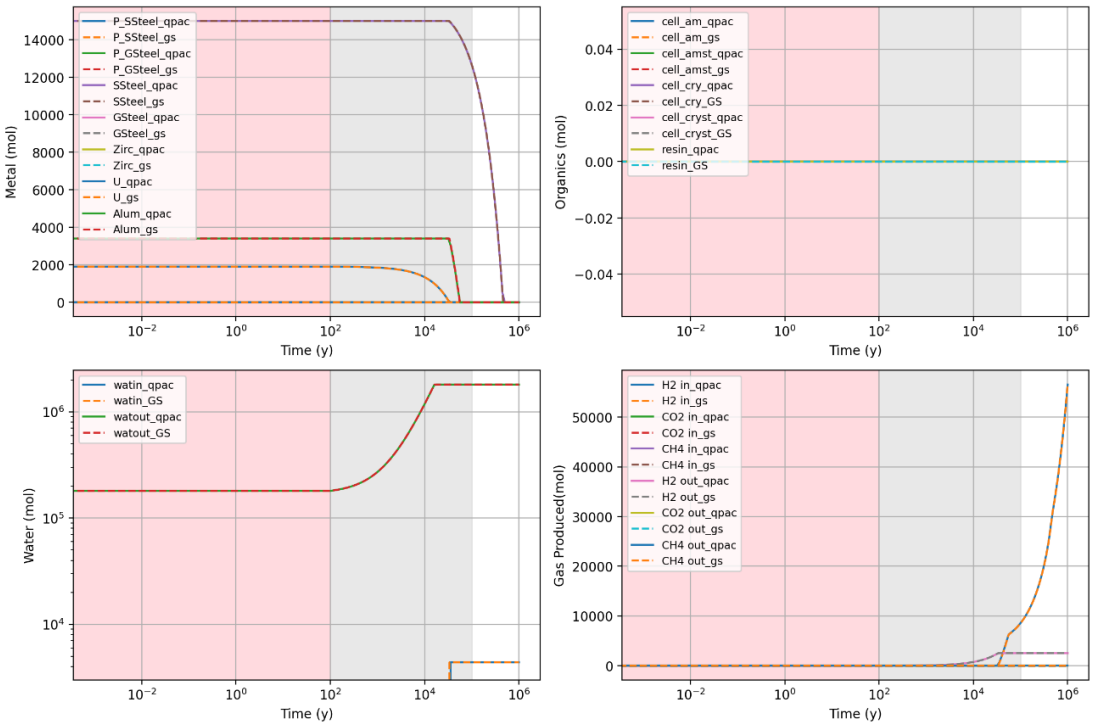

Figure D-3 Uranium Collection Filters: metals inventory (top-left); organics inventory (top-right); water inventory (bottom-left); and amounts of gas produced (bottom-right). (The results shown are for an earlier version of the central analysis case, as noted in the introduction to Appendix D.)

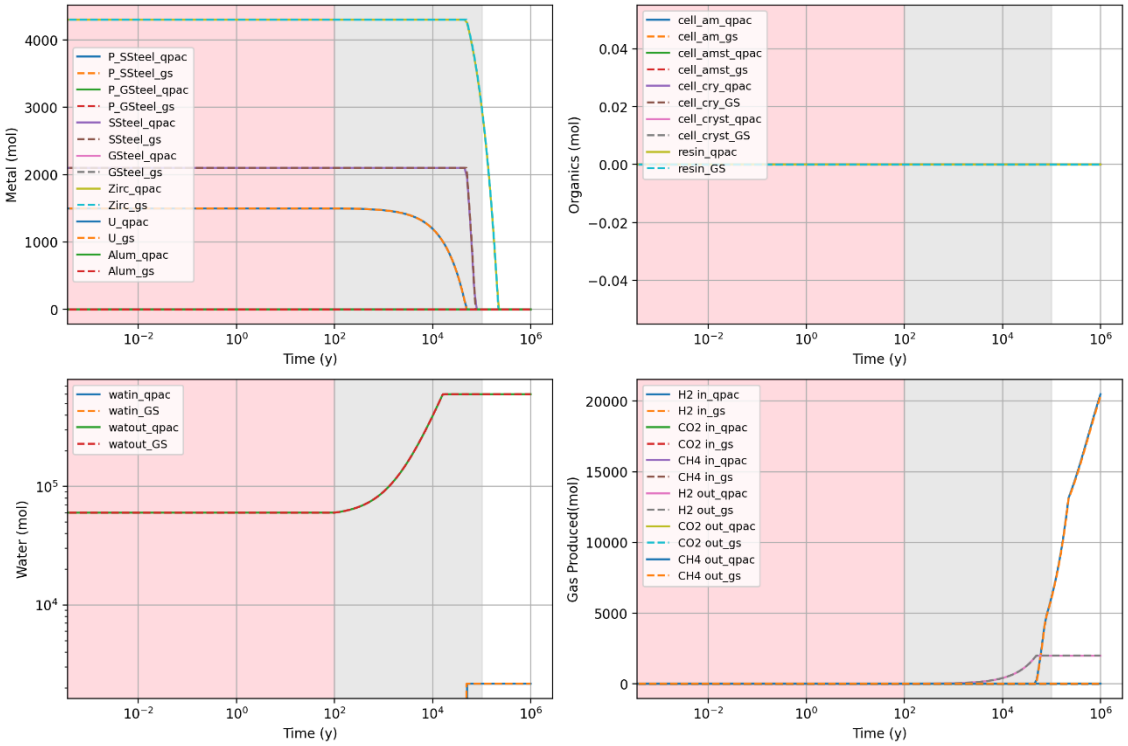

Figure D-4 Reprocessing Waste: metals inventory (top-left); organics inventory (top-right); water inventory (bottom-left); and amounts of gas produced (bottom-right).

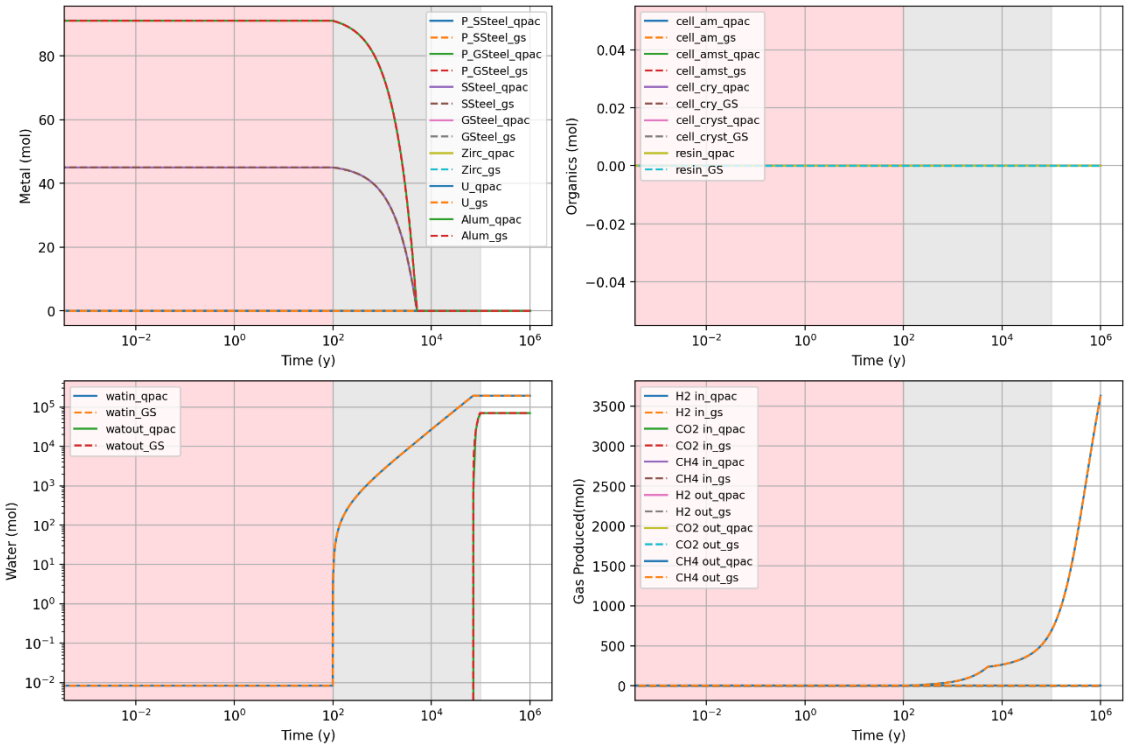

Figure D-5 Decommissioning Waste (Revised OPERA HLW Technical Waste): metals inventory (top-left); organics inventory (top-right); water inventory (bottom-left); and amounts of gas produced (bottom-right).

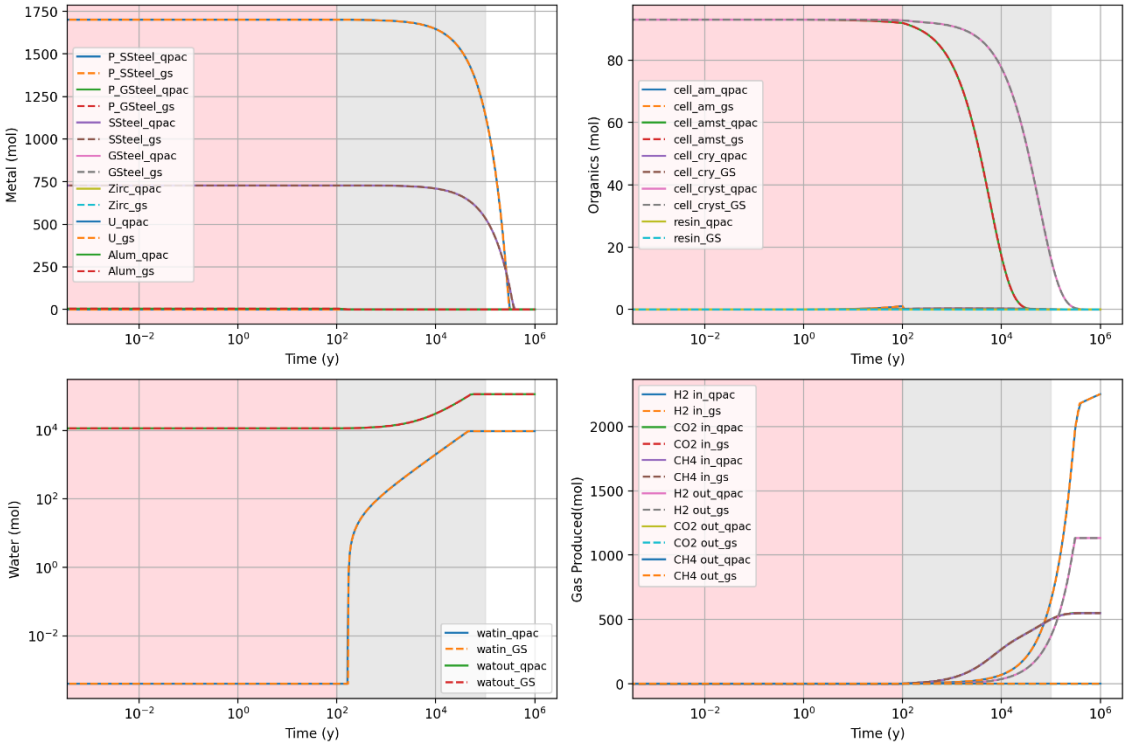

Figure D-6 Legacy Waste (Revised OPERA HLW Technical Waste): metals inventory (top-left); organics inventory (top-right); water inventory (bottom-left); and amounts of gas produced (bottom-right).

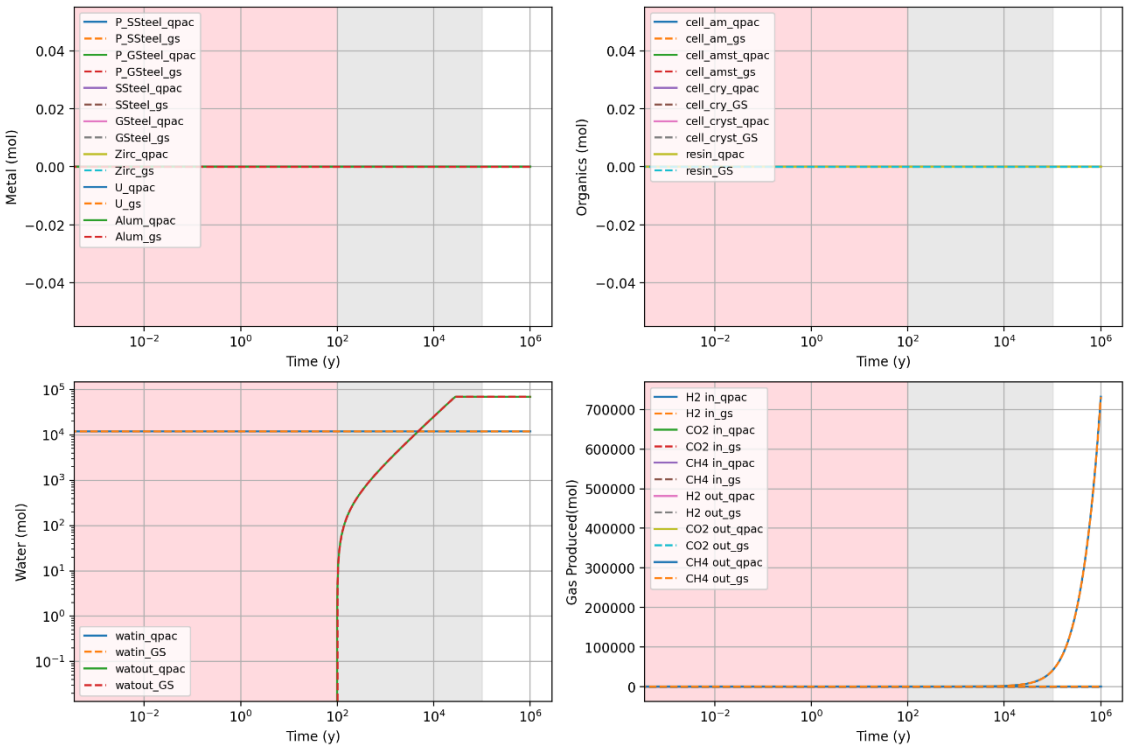

Figure D-7 Depleted Uranium: metals inventory (top-left); organics inventory (top-right); water inventory (bottom-left); and amounts of gas produced (bottom-right).

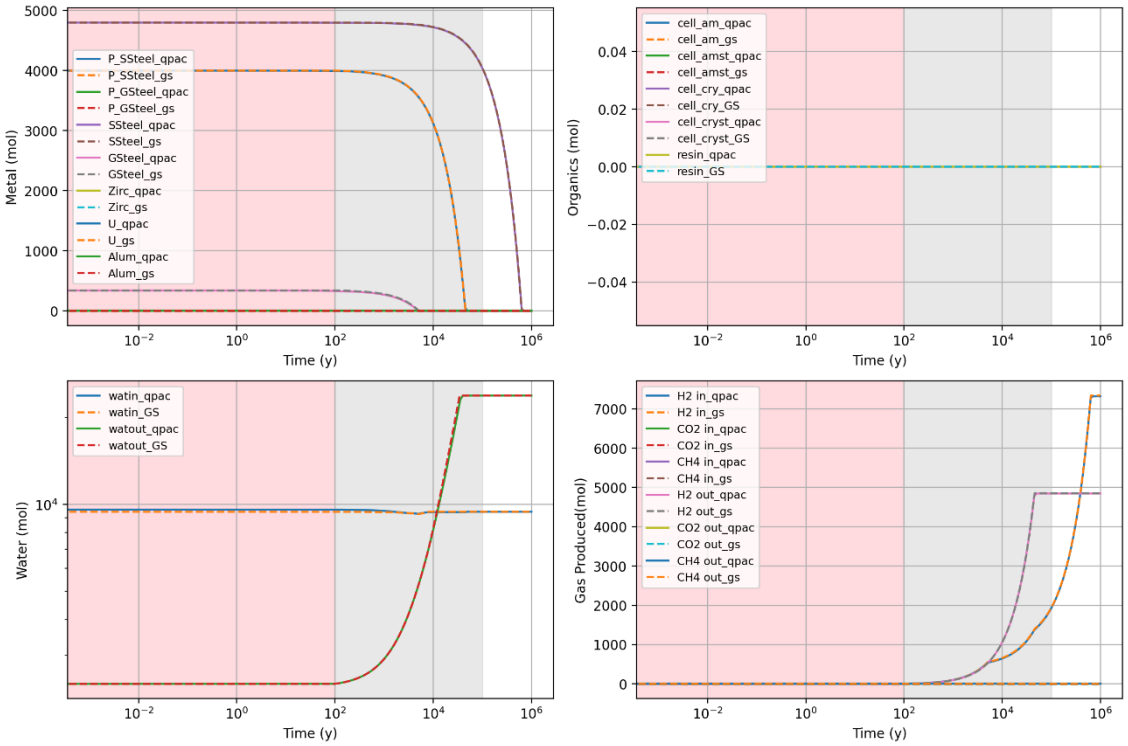

Figure D-8 Molybdenum Waste: metals inventory (top-left); organics inventory (top-right); water inventory (bottom-left); and amounts of gas produced (bottom-right). (The results shown are for an earlier version of the central analysis case, as noted in the introduction to Appendix D.)

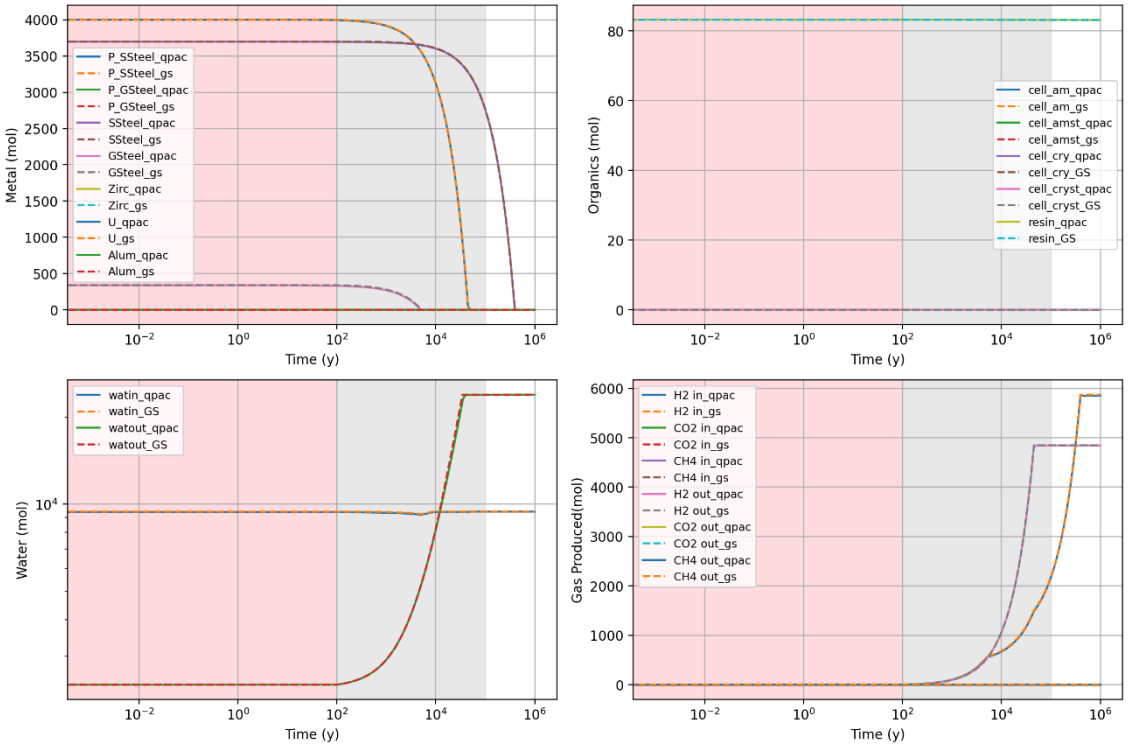

Figure D-9 Non-Compactible LILW: metals inventory (top-left); organics inventory (top-right); water inventory (bottom-left); and amounts of gas produced (bottom-

right). (The results shown are for an earlier version of the central analysis case, as noted in the introduction to Appendix D.)

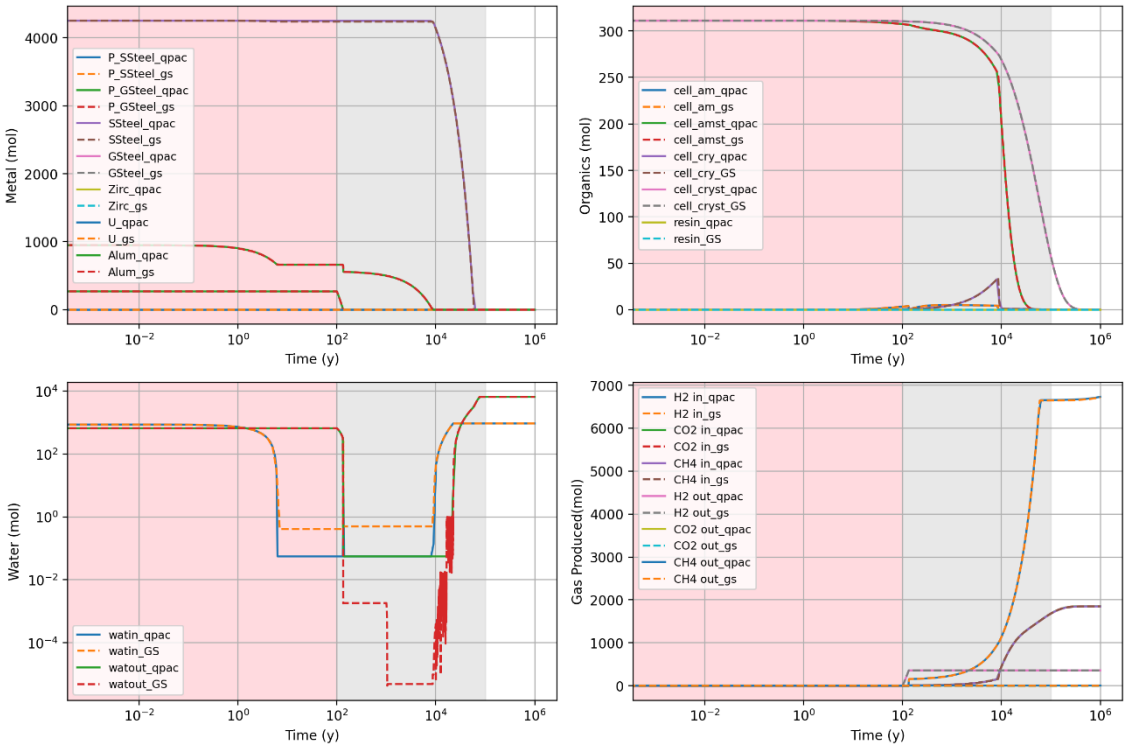

Figure D-10 Compactible LILW: metals inventory (top-left); organics inventory (top-right); water inventory (bottom-left); and amounts of gas produced (bottom-right).